https://doi.org/10.1016/j.jcsr.2021.106823

Effect of inter-module connections on progressive collapse behaviour of MiC structures

Xiao-Huang-Can He[a], Tak-Ming Chan[a,b*], Kwok-Fai Chung[a,b]

[a] Department of Civil and Environmental Engineering, The Hong Kong Polytechnic University, Hung Hom, Hong Kong, China

[b] Chinese National Engineering Research Centre for Steel Construction (Hong Kong Branch), The Hong Kong Polytechnic University, Hung Hom, Hong Kong, China

*Corresponding author: tak-ming.chan@polyu.edu.hk

Abstract

Modular Integrated Construction (MiC) is a game changing construction approach which could significantly increase construction efficiency, quality, and sustainability. For steel MiC structures, modules are manufactured in the factories and assembled at the construction sites through inter-module connections. The concern of the vulnerability of these connections under abnormal hazards leading to disproportionate progressive collapse will impede industrial applications of MiC structures in the construction community. This study investigates the structural robustness of corner-supported modular steel buildings with the focus on different inter-module connections. A sub-structure extracted from a five-storey module building is analysed by high fidelity finite element analysis under the corner column removal scenario. The load redistribution mechanism and failure modes are investigated thoroughly, based on which the simplified macro model is proposed where connections are modelled with rotational springs. Good consistence is found for the simplified model and the detailed FE analysis in terms of the pushdown curve. It is also found that the inter-module connection types will affect the beam-column joint properties which dominate the progressive collapse resistance of MiC structures. Therefore, attention should be paid when selecting different inter-module connections. The current rigid beam-column joint connection may lead to nonconservative evaluation.

Keywords: MiC structures; progressive collapse; inter-module connections, beam-column joint; failure modes; component approach

1 Introduction

Modular integrated Construction (MiC) structures were proposed several decades ago and were adopted for many applications among Hong Kong [1], mainland China [2], Korea [3], Singapore [4], Australia [5], UK [6], etc. Modules are manufactured in the factories under controlled circumstance and therefore quality is believed to be ensured. They are transported to the construction locations and assembled by cranes one by one. Noise can be significantly reduced, resources can be efficiently used, and construction wastes can be minimized. It is an innovative, clean, sustainable and environmentally friendly approach that could change the construction industry, especially in the high-density urban areas with serious aging issues.

Though successfully applied to many projects, concerns still exist about the reliability of connection systems [7] that could resist gravitational loadings, horizontal actions, and maintain stable under abnormal events. As a new structural type with complex connections between modular units through plates, bolts, shear keys, the safety of MiC structures must be carefully ensured and demonstrated. The structural response of MiC structures under gravitational loads using Vertorbloc connector connections were experimentally studied in Dhanapal et al. [8] and it was found that rigid beam-column joint property can be assumed during design. Chen et al. [9] and Chen et al. [10] experimentally studied the behaviour of a new type of inter-module connection under lateral loading and discussed the effect of welding quality and stiffeners on stiffness, strength and ductility. The global response of MiC structures under wind has also been discussed in [11, 12] while that under earthquake action can refer to [13-15], and the effect of connection properties on structural lateral behaviour was found to be significant. A comprehensive review on the MiC structural response under different actions and hazards, including transportation and construction loadings, ultimate strength design actions and service loadings can refer to Lacey et al. [16].

Studies on the progressive collapse behaviour of MiC structures are relatively few compared to other actions. To avoid the failure mode of "*house of cards*" as progressive collapse of Ronan Point building [17], it is vital to explore its structural performance under abnormal actions. Progressive collapse is a failure mechanism with extensive or total collapse of a building initiated by disproportionate small events or local damage [18]. Under key element or module removal scenarios, the collapse resistance of MiC structures should be provided both by modules and connections between modules. Aromaa et al. [19] experimentally studied the contribution of plaster-boarded wall inside modules to the integrity of a module itself through full scale test

using modules with and without infilled walls. The shear capability of the walls was also independently tested in [20]. Lawson et al. [20] studied the tensile demand of connections through simplified mechanical analysis based on force equilibrium. For design purpose, they recommended that the minimum horizontal force in any tie between the modules be taken as not less than 30% of the total load acting on the module. However, the suggestion was proposed based on an over-simplified model in which the module is suspended from its neighbours, which ignored the effect of flexural bending acting as cantilever mechanism. Similarly, Alembagheri et al. [21] studies the progressive collapse behaviour of MiC structures by numerical analysis, adopting rigid blocks for modules and only translational springs for connections. Therefore, failure of structures can only be induced by fracture of springs, rather than failure of modules, e.g. yielding of beams or failure of intra-module connections. Chua et al. [22] investigated the progressive collapse potential of a 40-storey steel frame MiC building, where horizontal connections were assumed fully rigid and vertical connections were assumed pinned. Results showed that the risk of progressive collapse is small. By analysing a five-storey MiC structure, Luo et al. [23] concluded that higher rotational stiffness and tensile resistance of inter-module connections could increase the collapse resistance.

Most of the above-mentioned studies focuses on only one inter-module connection type and therefore whether the findings can apply to MiC structures with other types of connection are questionable. Also, the beam-column joints within modules are usually assumed to be rigid for the sake of simplicity and the inter-module connections are assumed to be pinned, semi-rigid, or rigid. The complex interaction behaviour among the connection region is not fully understood.

Many different inter-module connections have been proposed in the past several years, either simple or complicated. The present study focuses on a typical class of inter-module connections, denoted as single rod/bolt connection and will be described in section 2.2, which have been proposed or adopted in [12, 24-28]. The common basic structural behaviour of these connections are to be investigated and discussed through high fidelity finite element analysis and simplified mechanical models. It is hoped that this study could help the understanding on how the inter-module connections affect the structural performance of the joint region and further affect the progressive collapse resistance of steel MiC structures, and more importantly how to improve the joint region to secure safety.

2 Structural design and analysis setting

2.1 Global structure

Hospitals and healthcare facilities are often constructed using modular construction, either for specialist rooms or as complete modular buildings [26]. Modular units used for the health sector are usually relatively large with partially or fully open sides. A five-storey 6×6 MiC structure is adopted as the studied structure (Figure 1). The building was assembled by a series of identical corner-supported modules with 5 m long, 3 m high and 3 m wide. The design nominal gravitational loads are shown in Table 1, where the dead load (G_k) consists of the self-weight of structural members and a superimposed dead load to account for the placement of utilities, floor finishes, etc. An extra beam line load equal to 5 kN/m is added to consider the effect of light weight infilled walls. The live load (Q_k) was taken as 2.0 kN/m^2 for floor slabs and zero for ceiling systems. The structure is assumed to be located in Hong Kong, where the main lateral action is wind load. The floor slabs were considered as typical concrete slab with a thickness of 100 mm. For each module, the designed section sizes for beams, columns and braces are shown in Table 2 with material grade S355, which are determined in ETABS [29] with the assumption that beam-column joints are rigid while column to column connections are pinned. The lateral stability is provided by a bracing system. X-braces made of two steel bars with angle section L120×10 are put on the middle modules at the perimeter of the building and inner modules inside the building from the bottom storey up to the top, as shown in Figure 1. The size of braces was determined to satisfy the lateral displacement requirement under wind loading in Hong Kong.

2.2 Connection systems

As shown in Table 2, hollow steel sections are adopted for both columns and beams. The intra-module, or beam-column connections feature with fully butt welded with enough strength, but without any reinforcement. As for inter-module connections, many types have been proposed by different researchers in the past decade. Comprehensive introduction of them can refer the several reviews papers, including Lacey et al. [30] with focus on bolted connection, Thai et al. [31] with focus on structural requirement, and Srisangeerthanan et al. [32] with focus on structural, manufacturing and construction performance. Among them, one class of connections adopts one single rod or bolt to vertically tie the upper and lower modules, as shown in Figure 2. The axial compressive force is transferred from the upper module to the lower module by the hollow steel section, while the possible axial tensile force is transferred solely by the single rod or bolt. The shear force among the modules can be resisted through adding a shear key, as shown

in Figure 2(a), (b), and (c), or simply resisted by the bolt itself, as shown in Figure 2 (d), (e), and (f). The moment resistance is provided by the coupling effect between the rod/bolt in tension and the one side of the columns in compression due to contact. The horizontal connection between modules can be realized through adding an intermediate plate, as shown in Figure 2 (c).

To study all the six connections shown in Figure 2 is too ambitious and faces the restriction due to lack of detailed information in some of the corresponding references. In the following section, four variants of the single rod/bolt connection mainly based on the connection shown in Figure 2(a) [25] and Figure 2(d) [26] are considered to apply to the above-designed MiC building structure shown in Figure 1, including two connections featuring with shear key connector and two with bolt connector. It is believed that the adopted connections can represent the major common features of this class of inter-module connections.

2.2.1 Shear key connection with or without column endplate

The first considered inter-module connection is an interlocking inter-module connection, as shown in Figure 2(a) proposed by Lacey et al. [25]. The proposed connection consists of a shear key combined with a tie rod located inside of the hollow steel sections for module columns. The shear key is made up of two square hollow section smaller than the module columns welded to a middle plate with a hole for the rod to pass through. Two plates are also welded inside the columns to hold on the tightening of the connecting rod, while a rectangular access hole is opened above the plates to install the rod at each column. Circular access holes could be opened instead to reduce the adverse effect on the resistance as much as possible [33]. These two plates also work as stiffeners for the beam-column joint region as they are aligned with the top flange of the floor beam or the bottom flange of the ceiling beam. The inner section view of the connection is also shown in Figure 3(a).

Based on preliminary analysis, it was found that the connection provided in [25] is rotationally weak since there is no strong horizontal support for the column face connected to the beams near the intermediate plate and yielding of the column face occurs first. To overcome the shortcoming, endplates are added to the column ends, and the size of the shear key is adjusted accordingly, as shown in Figure 3(b). A square hole is in the middle of the endplate to allow the shear key to pass through, which is somehow similar to the connection described in Figure 2(c) [12]. Better structural performance can be assumed if circular hollow section for the shear key is adopted and then the hole in the endplate is adjusted to circular [34].

2.2.2 Bolt connection with or without stiffeners

A single bolted vertical connection is described in Lawson et al. [26], as shown in Figure 2(d). The connection is accomplished by the bolt connecting the endplates of the top and bottom column through an intermediate connecting plate Figure 3(c). Usually access holes in the columns are required to tighten the bolts. No internal stiffeners are added in the columns. This connection is considered as the third connection to be analysed later.

The last connection considered is a bolted connection similar to the third connection. The only difference is that internal stiffeners in the columns at the level of beam flanges are added to enhance the beam-column joint region, as shown in Figure 3(d), which is somehow similar to the connection shown in Figure 2(f). It is noteworthy that the internal stiffeners in the tubular column is not desirable in terms of cost efficiency and field application because of the complication involved in the process of welding diaphragms to the hollow steel tube with closed cross-section [35]. Welding of internal diaphragms requires considerable skill [36]. Several fabrication processes are available for the internal stiffeners. For example, if the column is made of four steel plates vertically welded, the continuity plate can be welded after three-sides of column are attached, and the fourth dimension of column is performed later [37].

The four connections are labelled as “KS”, “KSE”, “BE”, “BSE”, respectively, to facilitate further demonstrations, where character “K”, “S”, “E”, “B” represent the shear key, stiffener, endplate, and bolt, respectively.

The above-described four connections are adopted for column-to-column connection at the external of the MiC building in the two-dimensional manner. It can be adjusted to fulfil the requirements for connection in internal connections and roof connections, as shown in Figure 4 for the “KS” case. Extension of the last three connections for internal and roof inter-module connections can refer to Figure 4, which is trivial and is not shown further.

3 Numerical analysis approach

Experimental test of progressive collapse of multi-storey modular buildings cannot be conducted easily due to the costly procedure and the required advanced facilities. Hence, the 3D finite element analysis approach is the most widely used method to study the behaviour of progressive collapse of structures. Key assumptions, FE modelling methodology, and loading and analysis procedure adopted in the present study for efficient analysis will be demonstrated in this section.

3.1 Key assumptions

3.1.1 Corner column removal scenario

To analyse progressive behaviour of buildings structures, there are usually two analysis approaches: threat-dependent approach and threat-independent approach [38]. Threat-dependent approach requires direct incorporating the initiating event such as gas explosion, vehicle impact, etc. during the mechanical analysis of the structure so that the whole process of structure behaviour can be demonstrated. However, the information of the events, such as equivalent amount of explosive materials, stand-off distance, impact velocity, contact surface area, etc. should be investigated first and it is uncertain about the exact values before the occurrence of the events. On the other hand, threat-independent approach allows notional removal of a key element inside the structure and then to assess the subsequent response of the structure under the gravitational loading. It is believed that as long as alternative load paths in the structure can be provided under key element removal scenarios, the structure can arrest progressive collapse under different kinds of initial hazards. Therefore, using threat-independent method can simplify the analysis process.

Columns in a building structures support the gravitational loading transferred from slabs and beams and therefore loss of a column would usually lead to more devastating consequence than removal of a beam or a part of slab. After the collapse of the twin towers of World Trade Center [39], General Services Administration [40] requires column removal as the design case for progressive collapse design of federal buildings, where corner columns, penultimate columns and external columns at the side of the layout of the building should be removed to check the collapse potential. He et al. [41] and Kim et al. [42] concluded that the external corner column is the most dangerous removal scenarios among others for concrete frame structures and steel frame structures, respectively. Therefore, a corner column removal scenario would be considered here and finite element analysis would be carried out to study the progressive collapse behaviour of MiC structures. In the finite element model, the corner column is notionally removed, while the joints at the top and bottom of the column are maintained intact, as shown in Figure 5.

3.1.2 Sub-structure model

The most accurate finite element analysis approach is three-dimensional nonlinear dynamic analysis of a structure given a sudden column removal scenario. However, nonlinear dynamic analysis is computationally cost-expensive. Nonlinear static analysis or pushdown analysis [43], where the specified gravitational loading at the damaged bays is increased gradually with a

proportion factor until failure, provides an alternative analysis approach. The nonlinear behaviour of the structure and the load re-distribution and resisting mechanisms can be straightforwardly identified by pushdown analysis. The maximum loading factor obtained from the pushdown analysis is the progressive collapse resistance of the structure.

However, even pushdown analysis of a whole MiC building structure with multiple spans and storeys is still very time-demanding. For progressive collapse analysis of a concrete bare frame structure, it was found that sufficient accuracy (error less than 5%) can be obtained when using a sub-structure located on the neighbouring one-bay region surrounded by the removed column [44] using solid elements. The difference is also negligible when slab is included in the analysis [41] where beam element for beams and columns, and shell elements for slabs were applied. Furthermore, it is also found that the collapse resistances are similar after removal of a column at different storeys along the height of a building if the structural design at each storey is similar (for example, the structural configuration and the superimposed loadings) [41], which is the case for steel MiC structure. Therefore, a two-storey substructure with one and a half bays were modelled as shown in Figure 5, which is sufficient to show the structural behaviour of the building against progressive collapse. The inter-module connections at the top are adjusted to the corresponding roof connections. To further simplify the analysis, only the planer frame is extracted from the building to study the effect of different inter-module connections on the load resisting mechanism and capacity of the structure in the context of progressive collapse. Three-dimensional effect due to the existence of slab and spatial effect should be investigated in future study.

3.2 FE model and validation

The FE model is analysed by ABAQUS [45] with solid elements for beams, columns and connections. The software has been adopted to simulate progressive collapse behaviour of beam-column sub-structure by other studies [46, 47]. The C3D8I element is adopted for all members since it can consider flexural deformation by using fewer number of elements compared to the C3D8R element in the thickness direction. The mesh size is between 4 to 200 mm, where it is finer around the joint region (Figure 6) and coarser at the middle of beams and columns. One element is adopted in the thickness direction for beams and columns. As for the material, Grade S355 steel was used for all the beams, columns, plates, and shear keys, and M8.8 bolts were adopted. Elastic-plastic with isotropic hardening property are adopted for all materials. General contacts were defined for the interfaces between the bolts, shear keys, beams, columns and

intermediate plates. Welds were modelled as tie constraints between different parts. A small force was imposed on the bolt to solve the convergence issue.

It should be noted no tests have been carried out for the four inter-module connections in the context of progressive collapse by the authors and others. Only the load-slip behaviour between the shear key and the intermediate plate in the horizontal direction had been tested for the KS connection by Lacey et al. [25], where the initial stiffness and the slip factor were studied. Figure 7(a) shows the joint configuration, and Figure 7(b) illustrates the experimental deformation and the simulated deformation using the modelling strategy discussed in this section. The experimental and simulated force-slip curves shown in Figure 7(c) for two specimens match well with each other in terms of initial stiffness and slip resistance, justifying the accuracy of the numerical model.

To further validate the finite element model, experimental tests of two inter-module connections designed and tested in Chen et.al [9] (external) and Chen et.al [10] (internal) under lateral loading were analysed, as shown in Figure 8. The configurations of the connections are shown in Figure 8(a). Hollow steel section was adopted for all the beams and columns. The vertical continuity is provided by the bolts at the end of beams with diameter equal to 24mm supported by three steel plates at the top, middle and bottom, respectively, while the horizontal continuity is provided by the shear key. Further detailed information about the specimens is shown in Figure 9 and Table 3. Both the two specimens were loaded with an axial compressive force equal to 0.2 times of the corresponding compressive capacity of the specimens first and then laterally pushed until failure, as shown in Figure 8(b). Using the similar setting of the material, element and meshing, finite element analysis was carried and the obtained deformation of the two specimens are shown in Figure 8(c). Lateral load-displacement curves obtained from the tests and simulations are also shown in Figure 8(d). The initial stiffness and yielding strength are well captured by the finite element analysis. The experimental curves demonstrated a decreasing trend after reaching the peak loading resistance due to cracking of the welding between the beams and columns. In the finite element model, damage of material/element was not defined and therefore such behaviour was not captured. Since in our connections welding is assumed to be strong enough and cracking will not occur, the finite element model is deemed to be sufficiently accurate for further analysis.

3.3 Loading and analysis procedure

During the analysis, the load combination is (specified in [48, 49])

$$G_k + 0.5Q_k \quad (1)$$

Half of the loads on the floor and ceiling levels are considered for the sub-structure. The boundary conditions at the ground level are fully fixed, while that the rightmost beam ends are rotationally pinned in the plane of the structure. It is assumed that the loads at each storey are solely resisted by the beams at the storey and therefore no extra load is added to the sub-structure transferred from the upper stories. And since the rotational stiffness of the column-to-column connection is relatively small compared to the hollow column section, no extra restraint is imposed on the top of the sub-structure.

Implicit dynamic analysis was carried where loads are gradually imposed on the beams at the first bay only due to convergence issue. And only the failure bays were loaded to explore the progressive collapse resistance of the structure. The vertical displacement of the point in the middle of the external floor joint above the removed column was recorded, as well as the loading factor α defined below

$$\alpha = Total\ Load/(G_k + 0.5Q_k) \quad (2)$$

where *TotalLoad* represents the total load applied on the structure. The analysis is stopped when the vertical displacement of the monitored node exceeds an allowable value. The criterion of $0.2L$ is specified in the tie force method in DoD [50], where L is the span length of a module, with the assumption that a tensile catenary action can be activated at relative large deformation, which can be interpreted as failure of beams or intra-module connections. However, in the current study, only corner column removal scenario is considered, and that no tensile catenary mechanism will be formed. The fracture of welding is not considered and it is unsure whether the weld is intact when the deformation is extremely large, as detected in some experimental tests [51]. Therefore, the allowable displacement is determined to be $0.1L$, which is believed to be large enough for the structure to develop fully plastic hinge at the members or joints. Here L is 5.0 m. Therefore, a vertical displacement of the node above the removed column equal to 0.5 m demonstrates failure.

4 Analysis results

4.1 Global deformation

Figure 10 shows the global deformation of the substructure at the final stage when using the shear key connection (KS) without endplate. The stress at the beams and columns are small. For example, the Mises stress at the topmost fiber at the middle of the ceiling beam at the second

storey is merely 55 MPa, and that at the one-fourth location is 120 MPa. By contrast, large stress and strain occur at around the joint region (355 MPa in the external roof joint region). The stress at the second half bay is very small and therefore is not shown in figure 10.

Figure 11 shows the pushdown curve (load-displacement curve) at the monitored node (shown in Figure 5) of the sub-structure, featuring with nearly bilinear behaviour. The sequence of yielding locations at the six beam-column joint region of the sub-structure is shown in Figure 10 and Figure 11. When the vertical displacement of the monitored node reaches at about 0.05m, yielding firstly occurs at the right floor beam-column joint region at the second storey (marked as ① in Figure 10). The criterion of yielding is defined as that the equivalent plastic strain (PEEQ) is larger than 0.001 in not less than 3 integration points in not less than four C3D8I solid elements to reduce the effect of premature assessment of yielding due to local effect. It signifies the end of elastic stage of a joint region rather that the fully strength stage. After the first yielding location, yielding occurs at the right ceiling beam-column joint region at the second storey (②) and then that of the first storey (③). Subsequently, yielding occurs at the left floor beam-column joint (④) and left ceiling beam-column joint region (⑤) at the second storey when the monitored displacement reaches about 0.1 m. The left ceiling beam-column joint at the first storey begins to yield (⑥) when the displacement reaches 0.2 m at the second branch of the nearly bilinear shape of the pushdown curve, demonstrating that the sub-structure enters the stage where stiffness is mainly provided by the hardening of the joint regions.

Figure 12 shows the pushdown curves for all the four connections considered. The collapse resistance at the failure criterion for the KS, KSE, BE, BSE connections are 0.45, 0.99, 0.58, and 0.90, respectively. It is observed that by adding endplates for the shear key connection or adding stiffeners for the bolted connection could significantly increase the collapse resistance. The detailed mechanisms will be explained in the next subsection.

4.2 Local deformation and failure modes

Figure 13 shows the local deformation at the external floor joint seen from outside and inside. For the KS connection, the stress localizes at the floor beam end and upper column side wall and face. For the floor beam-column joint, the plastic strain localizes at upper column face and the top of floor beam, due to a lack of horizontal resistance of the column face. Situation is similar for the ceiling beam-column joint. The strain in the shear key is very small and is not shown in Figure 13(a) to demonstrate the strain at the column face clearly. It can be found that the compressive force of the floor beam top flange produced by the beam end moment is resisted

by the stiffener, while the tensile force is transferred to the column face and then to the column side walls. The stiffness of the column face in bending is small, leading to large deformation on it. Apparent failure mode of column face in bending is shown. Fully strength of the floor beam cannot be accomplished.

For the KSE connection, the stress localizes at the floor beam end and the column side walls. The compressive force of the floor beam top flange produced by the beam end moment is resisted by the stiffener, while the tensile force is transferred to the column end plate and then to the column side walls. The plastic strain localizes at the floor beam ends at top flange due to the compression force and at bottom flange due to the tensile force. Therefore, the beam flexural strength can be realized, and the failure mode is beam end yielding. The bolt is in large tension and it yields at the two ends due to local effect, signifying the bolt in tension failure mode.

For the BE connection, three possible failure modes can be detected. Firstly, due to lack of stiffeners at the level of beam top flange, the compression force produced by the top flange of the floor beam leads to significant bending deformation of column face, showing large plastic strain at that location. Situation is similar for the ceiling beam-column joint. Secondly, stress localizes around the access hole at the front column side wall, leading to potential shear failure of the column side walls. Thirdly, the connecting bolt yields due to the tensile force.

For the BSE connection, the stress localizes at the top floor beam end, as well as the column side walls. The plastic strain localizes at the floor beam ends at both top and bottom flanges. The strain at the intact column side wall is also large, signifying that column side wall is in shear yielding stage. The bolt is in large tension and it yields, signifying the bolt in tension failure mode.

The local deformation of the joint region at different locations for connection KS is shown in Figure 14. All the failure modes are column face in bending. Relative horizontal displacement of the column-column connection is also observed due to the tolerance between the bolts and holes and that between columns and shear keys as shown in Figure 14(d). Yielding even starts to occur at the end of the bolts for the connections between the first floor and second floor. The strain in the horizontal connecting plates is small. Similar findings are also observed in other three types of connections and therefore their local deformation is not shown here.

It should be noted that European Committee for Standardization [52] lists several failure modes for hollow section joints, including (a) chord face failure, (b) chord side wall failure by yielding, crushing, or instability, (c) chord shear failure, (d) punching shear failure, (e) brace

failure, (f) local buckling at the joint location, where the chord and brace member can be interpreted as column and beam here. Some of them are not observed in the FE analysis due to the modelling assumptions and parameter setting. The observed failure modes at the joint region for the four inter-module connections are summarized in Table 4.

4.3 Load resisting mechanism

Based on the global and local deformations, the load resisting mechanism is shown in Figure 15. The total overturning moment relatively to the point *O* shown in the figure is resisted by two parts, cantilever beam mechanism and Vierendeel mechanism [53, 54]:

$$\frac{QL}{2} = M_{beam} + M_{viereendeel} = \left(M_{cb,1} + M_{fb,2} + M_{cb,2}\right) + T_{cb,2}H \tag{3}$$

where $M_{cb,i}$ and $M_{fb,i}$ represent the moment resistance of the right end of the ceiling beam and floor beam at the i-th storey, including the with consideration of the potential partial strength of joints; and $T_{cb,i}$ and $T_{fb,i}$ represent the tensile force of the right end of the ceiling beam and floor beam at the i-th storey. The second part of the right-hand side of Eq. (3) is induced by the Vierendeel effect of the beams and columns intersecting to each other at the left part of the sub-structure, and its magnitude is controlled by the strength of the ceiling beam-column joint, floor beam-column joint, and the column-column connection. Thus, the total collapse resistance is provided by all the beam-column joints and column-column connections.

It should be noted that six hinges are enough to form a geometrical unstable mechanism for the left part of the structure shown in Figure 15. The formation of the three plastic hinges at the right end of the three beams and the two plastic hinges at the left end of the beams at the second storey are predictable. Due to the small distance between the column-column connection and the ceiling beam-column joint immediately above the removed column, only one of them which shows smaller strength would fail. Therefore, a total number of six plastic hinges would occur at the final failure stage. The total load that the sub-structure can hold can be estimated by

$$Q = 2\left(\min\left(M_{cb,1}, M_{cc}\right) + M_{cb,1} + 2M_{cb,2} + 2M_{fb,2}\right)/L \tag{4}$$

where M_{cc} is the moment resistance of the column-column connection.

4.4 Contact of double beams

It is theoretically difficult to estimate the contact effect between the middle two beams. It depends on the one hand on the sectional stiffness of the two beams and the corresponding loads, on the other hand, it also depends on the rotational angles at the joint regions at the two ends.

According to the solid element model, the contact normal and frictional forces between the middle two beams are small. The maximum contact stress is 6.3 MPa (Figure 16). Eliminating the interaction definition between the bottom face of the floor beam at the second storey and the upper face of the ceiling beam at the first story leads to almost the same collapse resistance at the allowable displacement, although the two beams do intersect to each other with the maximum value equal to about 20 mm. The difference of collapse resistance is smaller than 1%. Progressive collapse resistance is not significantly changed because of contact between beams.

The phenomenon can be explained as follows: If a point load is imposed on the monitored node until that large plastic deformation occurs at the beam ends, the two beams behave like two straight lines as the plastic rotational angles at the end of the two beams are equal. Since distributed loads are imposed on both the ceiling beam and floor beam, and the ratio of relative deflection $(q_{fb}L^4/EI_{fb})/(q_{cb}L^4/EI_{cb})$ is equal to 1.62 which is larger than 1.0, representing that the deflection of the floor beam is larger than the ceiling beam, where q is the distributed load, subscripts $_{fb}$ and $_{cb}$ refer to floor beam and ceiling beam, respectively. When the difference of the deflection is over the gap between the two beams (10 mm in the study), the local contact force would push the ceiling beam downward and contact stress is produced. However, due to the weak stiffness of the joints after yielding, the contact stress is small.

5 Simplified model

High fidelity finite element analysis requires enormous simulation effort, and it is computationally impractical for full large structures for everyday design. It is necessary to propose simplified macro model for quick assessment of structural behavior and collapse resistance under column removal scenarios based on potential failure modes. In this section modelling approaches for the failure modes listed in Table 4 will be presented. The relative horizontal displacement between upper and lower columns due to the tolerance is not considered for the sake of simplicity, which requires further study in the future.

Figure 17 shows the simplified model proposed featuring with the floor beam-column joint, ceiling beam-column joint and column-column connection. Both the beam-column joint can incorporate a series of components representing the failure models observed in the detailed finite element analysis, since their effect is significant based on the local deformation from FE analysis. Other components not shown in Table 4 could also be included to provide better simulated results.

Bilinear behavior is assumed for all the components with the properties of initial stiffness and yielding resistance. Due to the irregular shape, some of the properties of the components are

not provided in EN 1993-1-8 [52]. Mechanisms to calculate these properties are demonstrated in the following subsections.

5.1 Shear key connection without endplate (KS)

The geometrical information of the connection is shown in Figure 18, where the sectional height, sectional width, thickness of the tube of the column and beam are h_0, h_1, b_0, b_1, t_0, t_1, respectively.

5.1.1 Column side walls in shear

Although the failure mode column side walls in shear (cws) is not observed in the finite element analysis for the structure with KS connection, the model to estimate the moment resistance of the failure mode is still provided for comparison with other connections. The model for the column side wall shear component is shown in Figure 19(a), which is similar to the column web shear component for I sections [55]. The shear area A_v is approximated as

$$A_v = 2(h_0 - t_0)t_0 \tag{5}$$

The rotational strength is

$$M_{cws} = \frac{A_v f_y (h_1 - t_1)}{\sqrt{3}} \tag{6}$$

where f_y is the yielding stress of the steel material and it is assumed to be the same for all the structural parts here. The rotational stiffness of the shear panel zone is approximated as [55]

$$K_{cws} = GA_v(h_1 - t_1) \tag{7}$$

where G is the shear modulus of the steel material.

5.1.2 Column face in bending

The yielding line mechanism in the column face in bending component is shown in Figure 18. Denote $\beta=b_1/b_0$, $\eta=h_1/b_0$, and the moment capacity per unit of the column and beam plate are m_0 and m_1, respectively, the internal dissipated energy for each yielding line (number shown in Figure 18) is shown in Table 5.

The total dissipated energy is

$$E_T = m_0\delta\left(\frac{1+\beta m_1/m_0}{\eta} + \frac{8\eta}{1-\beta}\right) \tag{8}$$

The external work done by the moment is

$$W = M\frac{\delta}{h_1} \tag{9}$$

Equating Eq. (8) and (9), the moment is obtained as

$$M = m_0 h_1 \left(\frac{1 + \beta m_1/m_0}{\eta} + \frac{8\eta}{1-\beta} \right) \quad (10)$$

The moment capacity per unit can be calculated as $m = f_y t_0^2/4$.

Calculation of the initial stiffness based on the elastic thin slab theory is very difficult. Here an alternative approach is adopted. The axial stiffness of a small rectangular plate to a larger long plate with two opposite sides being fixed (Figure 20) due to tensile force perpendicular to the larger plate can be calculated as [56]

$$k_{axail} = \frac{E t_0^3}{b_0^2} 16 \frac{t_1/b_0 + (1-\beta)\tan\theta}{(1-\beta)^3 + 10.4(1.5 - 1.63\beta)/(b_0/t_0)^2} \quad (11)$$

where θ can be estimated as 35-10β [56]. For the current connection KS, the bottom part of the cfb component can be seen as half of the part in [56]. Therefore, the axial stiffness is assumed to be half of the value in (11) and the rotational stiffness is calculated as

$$K_{cfb} = 0.5 k_{axail} (h_1 - t_1)^2 \quad (12)$$

by assuming that the axial stiffness of the connection between the column and beam upper flange is infinite due to the stiffener in the column.

The aggregated strength of the beam-column joint is

$$M = \min\{M_{cws}, M_{cfb}\} \quad (13)$$

And the stiffness of the connection is

$$K = \frac{1}{\frac{1}{K_{cws}} + \frac{1}{K_{cfb}}} \quad (14)$$

5.1.3 Column-column connection

The bolt in tension failure mode of the column-column connection can be modelled by a rotational spring induced by the bolt and the contacting effect between column ends and the intermediate plate. The stiffeners are designed to be relatively strong so that failure only occurs at the bolt. Thus, the moment capacity is calculated as

$$M_{VC} = f_{yb} A_b (h_0 - t_0)/2 \quad (15)$$

where f_{yb} and A_b are the yielding strength and area of the bolt. And the stiffness is calculated as

$$K_{VC} = k_b [(h_0 - t_0)/2]^2 \quad (16)$$

where k_b is the stiffness of the spring representing the bolt, which should include the deformation of the bolt itself as well as the flexural bending of the supporting plates. Since the supporting plates were designed very strong, only the bolt deformation is considered. It is calculated as

$$k_b = EA_b/L_b \tag{17}$$

where E is the elastic modulus, and L_b is the length of the bolt.

5.2 Shear key connection with endplate (KSE)

For the shear key connection with endplates, the column side walls in shear component are similar to the connection KS and therefore the strength and stiffness is calculated as per Eq. (6) and (7), respectively. Since there are stiffeners at both the top and bottom beam flange levels, effect of the column face in bending component can be eliminated in the model. The aggregated joint properties are that of the cws component. Properties of the vertical column-column connection is assumed to be the same specified in Eq. (15)~(16).

5.3 Bolt connection without stiffener (BE)

5.3.1 Column side walls in shear (cws)

The properties of column side walls in shear component can be obtained in section 5.1.1 by Eq. (6) ~(7). The effect of holes in the column side walls is assumed to be considered by only changing the shear area to

$$A_v = (h_0 - t_0 - d)t_0 + (h_0 - t_0)t_0 \tag{18}$$

where d is the width of the holes, as shown in Figure 19(b).

5.3.2 Column face in bending

The strength of cfb component can be determined by the yielding line mechanism shown in Figure 21. The internal dissipated energy for each yielding line (number shown in Figure 21) is shown in Table 6.

The total energy is

$$E_T = m_0\delta\left(\frac{4\tan\alpha}{1-\beta} + 4\cot\alpha + \frac{8\eta}{1-\beta} + \frac{2}{\eta}\right) \tag{19}$$

The external work done by the moment is

$$W = M\frac{\delta}{h_1} \tag{20}$$

Equating Eq. (19) and (20), the moment is obtained as

$$M_{cfb} = m_0 h_1\left(\frac{4\tan\alpha}{1-\beta} + 4\cot\alpha + \frac{8\eta}{1-\beta} + \frac{2}{\eta}\right) \tag{21}$$

where $\tan\alpha = \sqrt{1-\beta}$ when taking the minimum of Eq.(21). The moment capacity is

$$M_{cfb} = m_0 h_1\left(\frac{8}{\sqrt{1-\beta}} + \frac{8\eta}{1-\beta} + \frac{2}{\eta}\right) \tag{22}$$

The stiffness of cwb can be determined as follows. The axial stiffness of a rectangular plate to rectangular hollow section can be calculated as Eq. (11) [56]. Since there is an endplate for the BE connection to provide strong support, the rotational stiffness can be calculated as

$$K_{cfb} = k_{axail}(h_1 - t_1)^2 \quad (23)$$

which is twice to the value of connection KS as shown in Eq. (12). The aggregated strength and stiffness can be calculated according to Eq. (13)~(14).

5.3.3 Column-column connection

The column-column connection is similar to the connection type KS, except that the length of the bolt is relatively shorter, which is taken as the sum of the thickness of the intermediate plates and column endplates. Therefore, the properties can be obtained according to Eq. (15) ~(16). However, it should be noted that the shear force in the bolt may reduce the tensile resistance of the bolt and therefore reducing the moment resistance of the column-column connection.

5.4 Bolt connection with stiffener (BSE)

For the bolt connection with stiffener connection, the column side walls in shear component are similar to the connection BE and therefore the strength and stiffness is calculated as per Eq. (6) and (7), respectively. Since there are stiffeners at both the top and bottom beam flange levels, effect of the column face in bending component can be eliminated in the model. The aggregated joint properties are that of the cws component. Properties of the vertical column-column connection is assumed to be the same specified in Eq. (15)~(16).

5.5 Analysis results

Using the simplified model, the rotational resistance and stiffness are calculated, and the results are summarized in Table 7, as well as the relative stiffness and strength against the corresponding beam element. The detailed calculation process is also shown in the appendix A. For the connection KS, the moment resistance for the floor beam-column and ceiling beam-column joints are 0.32 and 0.29 times the corresponding member resistance, representing that failure would occur at the joint regions while the members remain almost elastic. The moment resistances of the beam-column joints are over the member resistance for the connection KSE, indicating that failure would occur at the member end. The stiffness of the joints in terms of the relative beam stiffness *EI*/*L* is also presented.

According to Table 7, for the external floor joint region near the monitored node, failure would occur at the ceiling beam-column joint for connection KS and BE, and at the column-column connection for connections KSE and BSE, due to the relative magnitudes of moment resistances. This matches well with the location deformation observed in the solid model (Figure 13), except for the connection BE. However, it is interesting that for the connection BE the calculated moment resistance of the ceiling beam-column joint is 12.0 kN-m, slightly lower than 13.3 kN-m of the vertical column-column connection, which means that failure should occur at the ceiling beam-column joint rather than the bolt shown Figure 13(c). This might be due to that the resistance for the latter is overestimated because of ignorance of the shear stress in the bolt, which could reduce the moment resistance of the column-column connection. The degree of the reduction requires further study.

The pushdown curve obtained by the simplified model for connection KS is shown in Figure 22, with comparison of the curve obtained by solid elements. The initial stiffness of the curve and the yielding strength of the sub-structure obtained from the simplified model match well with that from solid model. The yielding locations in the simplified model occur later than the solid model because the former demonstrates full plastic resistances while the later presents elastic resistances. The post-yielding strength of the sub-structure is underestimated by the simplified model partly due the underestimation of the hardening effect of the beam-column joints due to tensile membrane mechanism of column faces.

The pushdown curves obtained by the simplified model for the other three connections are shown in Figure 23. Good consistence is found compared to solid model and simplified model. Hence although the axial flexibility in the beams and the vertical inter-module connection are not considered, the simplified model can be adopted for quick assessment of progressive collapse of MiC structures under corner column removal scenarios.

Conclusion

A two-storey sub-structure was extracted in a modular steel building structure to comprehensively study the progressive collapse behaviour and resistance of MiC structures with different types of connections. High fidelity finite element analysis was carried out first to investigate the global deformation and especially the local failure modes. Simplified models were then proposed based on the observed failure modes for the considered connections, and they were incorporated to the macro model for progressive collapse analysis. It was found that the macro model with beam elements for beams and columns and rotational springs for joint

regions shows good consistence with the detailed FE analysis in the context of progressive collapse.

The inter-module connections have significant influence on the collapse resistance of MiC structures through the effect on the beam-column joints. The traditional assumed rigid beam-column joint assumption may lead to unsafe conclusion if they in fact show non-rigid behaviour. Adding endplates or stiffeners could enhance the joint region and therefore increase the collapse resistance.

It should be noted very basic models for different failure modes at the joint region in section 5 are adopted. Corresponding calculation formulas for stiffness and strength require further comprehensive parametric studies and experimental tests to verify. More components could be incorporated, and better post yielding mechanism can be considered to obtain more sophisticated results. The rotational capacity is not considered due to lack of experimental data.

Acknowledgement

The authors sincerely acknowledge the support from the Innovation and Technology Fund - Nano and Advanced Materials Institute (ITF-NAMI) for the project “Hong Kong Modular Integrated Construction (MiC) Innovations” (PolyU/ ZS12) and from the Chinese National Engineering Research Centre for Steel Construction (Hong Kong Branch) at The Hong Kong Polytechnic University.

Reference

[1] Construction industry council. InnoCell. 2010.

[2] Luo H, Liu J, Li C, Chen K, Zhang M. Ultra-rapid delivery of specialty field hospitals to combat COVID-19: Lessons learned from the Leishenshan Hospital project in Wuhan. Automation in Construction. 2020;119:103345.

[3] Park HK, Ock J-H. Unit modular in-fill construction method for high-rise buildings. KSCE Journal of Civil Engineering. 2015;20:1201-10.

[4] Chain P. Prefabricated prefinished volumetric construction (PPVC) in Singopore: NTU case studies. International Conference on Modular Integrated Construction. Kowloon, Hong Kong 2018.

[5] Gunawardena T, Karunaratne R, Mendis P, Ngo T. Prefabricated Construction Technologies for the Future of Sri Lanka’s Construction Industry. The 7th International Conference on Sustainable Built Environment. Kandy, Sri Lanka 2016.

[6] Lawson RM, Ogden RG, Bergin R. Application of modular construction in high-rise buildings. Journal of Architectural Engineering. 2012;18 148-54.

[7] Ferdous W, Bai Y, Ngo TD, Manalo A, Mendis P. New advancements, challenges and opportunities of multi-storey modular buildings – A state-of-the-art review. Engineering Structures. 2019;183:883-93.

[8] Dhanapal J, Ghaednia H, Das S, Velocci J. Behavior of thin-walled beam-column modular connection subject to bending load. Thin-Walled Structures. 2020;149.
[9] Chen Z, Liu J, Yu Y, Zhou C, Yan R. Experimental study of an innovative modular steel building connection. Journal of Constructional Steel Research. 2017;139:69-82.
[10] Chen Z, Liu J, Yu Y. Experimental study on interior connections in modular steel buildings. Engineering Structures. 2017;147:625-38.
[11] Lacey AW, Chen W, Hao H, Bi K. Numerical Study of the Structural Response to Wind Loading: Modular Building Case Study. 13th International Conference on Steel, Space and Composite Structures 2018.
[12] Chua YS, Liew JYR, Pang SD. Modelling of connections and lateral behavior of high-rise modular steel buildings. Journal of Constructional Steel Research. 2020;166:1-17.
[13] Lacey AW, Chen W, Hao H, Bi K. Structural Response of Modular Building Subjected to Earthquake Loading. 13th International Conference on Steel, Space and Composite Structures 2018.
[14] Gunawardena T. Behaviour of prefabricated modular buildings subjected to lateral loads 2016.
[15] Fiorino L, Macillo V, Landolfo R. Shake table tests of a full-scale two-story sheathing-braced cold-formed steel building. Engineering Structures. 2017;151:633-47.
[16] Lacey AW, Chen W, Hao H, Bi K. Structural response of modular buildings – An overview. Journal of Building Engineering. 2018;16:45-56.
[17] Griffiths H, Pugsley A, Saunders O. Report of the inquiry into the collapse of flats at Ronan Point, Canning Town; presented to the Minister of Housing and Local Government London, England: Her Majesty's Stationery Office; 1968.
[18] Starossek U. Progressive collapse of structures. London: Thomas Telford; 2009.
[19] Aromaa P, Sääksvuori O, Lawson M, Ogden R, Popo-Ola SO, Hekkanen M. Demonstration of modular construction in the renovation of existing concrete and masonry buildings. Brussels: Report EUR 20595 of European Commission, Technical Steel Research; 2003.
[20] Lawson PM, Byfield MP, Popo-Ola SO, Grubb PJ. Robustness of light steel frames and modular construction. Proceedings of the Institution of Civil Engineers - Structures and Buildings. 2008;161:3-16.
[21] Alembagheri M, Sharafi P, Hajirezaei R, Samali B. Collapse capacity of modular steel buildings subject to module loss scenarios: The role of inter-module connections. Engineering Structures. 2020;210:110373.
[22] Chua YS, Liew JYR, Pang SD. Robustness of Prefabricated Prefinished Volumetric Construction (PPVC) High-rise Building. Proceedings 12th international conference on Advances in Steel-Concrete Composite Structures - ASCCS 20182018.
[23] Luo FJ, Bai Y, Hou J, Huang Y. Progressive collapse analysis and structural robustness of steel-framed modular buildings. Engineering Failure Analysis. 2019;104:643-56.
[24] Sanches R, Mercan O, Roberts B. Experimental investigations of vertical post-tensioned connection for modular steel structures. Engineering Structures. 2018;175:776-89.
[25] Lacey AW, Chen W, Hao H, Bi K, Tallowin FJ. Shear behaviour of post-tensioned inter-module connection for modular steel buildings. Journal of Constructional Steel Research. 2019;162:105707.
[26] Lawson M, Ogden R, Goodier C. Design in modular construction: CRC Press; 2014.
[27] Liu Y, Chen Z, Liu J, Bai Y, Zhong X, Wang X. Lateral stiffness evaluation on corner-supported thin walled modular steel structures. Thin-Walled Structures. 2020;157:106967.

[28] Dai X-M, Zong L, Ding Y, Li Z-X. Experimental study on seismic behavior of a novel plug-in self-lock joint for modular steel construction. Engineering Structures. 2019;181:143-64.
[29] CSi. CSi analysis reference mannual - ETABS Integrated Building Design Software. Computer & Structures Incoporation, Berkeley, USA2016.
[30] Lacey AW, Chen W, Hao H, Bi K. Review of bolted inter-module connections in modular steel buildings. Journal of Building Engineering. 2019;23:207-19.
[31] Thai H-T, Ngo T, Uy B. A review on modular construction for high-rise buildings. Structures. 2020;28:1265-90.
[32] Srisangeerthanan S, Hashemi MJ, Rajeev P, Gad E, Fernando S. Review of performance requirements for inter-module connections in multi-story modular buildings. Journal of Building Engineering. 2020;28:101087.
[33] Singh, TG, Chan TM. Effect of access openings on the buckling performance of square hollow section module stub columns. Journal of Constructional Steel Research. 2021;177:106438.
[34] Doung P, Sasaki E. Load-deformation characteristics and performance of internal diaphragm connections to box columns. Thin-Walled Structures. 2019;143:106221.
[35] Kim S-H, Choi S-M. Tensile strength and concrete cone failure in CFT connection with internal diaphragms. International Journal of Steel Structures. 2017;17:643-52.
[36] Kurobane Y, Packer JA, Wardenier J, Yeomans N. Design guide for structural hollow section column connections: CIDECT; 2004.
[37] Rezaifar O, Younesi A. Experimental study discussion of the seismic behavior on new types of internal/external stiffeners in rigid beam-to-CFST/HSS column connections. Constr Build Mater. 2017;136:574-89.
[38] Haberland M, Starossek U. Progressive collaspe nomenclature. Structures 2009: Don't Mess with Sructural Engineerings: ASCE; 2009. p. 1886-95.
[39] National Institute of Standards and Technology(NIST). Final report on the collapse of the World Trade Center Towers. Principal Findings. 2005;175:1-6.
[40] General Services Administration. Alternate path analysis and design guidelines for progressive collapse resistance. 2016. p. 1-E44.
[41] He X-H-C, Yuan X-X, Yi W-J. Irregularity index for quick identification of worst column removal scenarios of RC frame structures. Engineering Structures. 2019;178:191-205.
[42] Kim J, Kim T. Assessment of progressive collapse-resisting capacity of steel moment frames. Journal of Constructional Steel Research. 2009;65:169-79.
[43] Khandelwal K, El-Tawil S. Pushdown resistance as a measure of robustness in progressive collapse analysis. Engineering Structures. 2011;33:2653-61.
[44] Botez M, Bredean L, Ioani AM. Improving the accuracy of progressive collapse risk assessment: Efficiency and contribution of supplementary progressive collapse resisting mechanisms. Computers & Structures. 2016;174:54-65.
[45] Dassault Systèmes. ABAQUS Documentation. Providence, RI, USA 2019.
[46] Dinu F, Marginean I, Dubina D. Experimental testing and numerical modelling of steel moment-frame connections under column loss. Engineering Structures. 2017;151:861-78.
[47] Alrubaidi M, Elsanadedy H, Abbas H, Almusallam T, Al-Salloum Y. Investigation of different steel intermediate moment frame connections under column-loss scenario. Thin-Walled Structures. 2020;154:106875.
[48] CECS392. Code for anti-collapse design of building structures. China Planning Press; 2014.
[49] European Committee for Standardization. Eurocode - Basis of structural design (EN 1990:2002+A1). CEN (European Commitee for Standardization); 2005.

[50] Department of Defense. Design of buildings to resist progressive collapse (UFC 4-023-03). Washington, D.C.2016.
[51] Deng E-F, Zong L, Ding Y, Dai X-M, Lon N, Chen Y. Monotonic and cyclic response of bolted connections with welded cover plate for modular steel construction. Engineering Structures. 2018;167:407-19.
[52] European Committee for Standardization. Eurocode 3: Design of steel structures - Part 1-8: Design of joints (EN 1993-1-8: 2005). CEN (European Commitee for Standardization); 2006.
[53] Sagiroglu S, Sasani M. Progressive Collapse-Resisting Mechanisms of Reinforced Concrete Structures and Effects of Initial Damage Locations. Journal of Structural Engineering. 2014;140:04013073.
[54] Qiao H, Yang Y, Zhang J. Progressive Collapse Analysis of Multistory Moment Frames with Varying Mechanisms. Journal of Performance of Constructed Facilities. 2018;32:04018043.
[55] Faella C, Piluso V, Rizzano G. Structural steel semirigid connections: theory, design, and software: CRC press; 2000.
[56] Costa Neves L, Gomes F. Semi-rigid behaviour of beam-to-column minor-axis joints. 1996.

Appendix A Worked examples about the calculation of the connection properties

Detail calculation of joint properties for the four types of connection is shown in this section. Only the information of connection KS and BE is presented, since the corresponding KSE and BSE connection are similar and even easier to obtain.

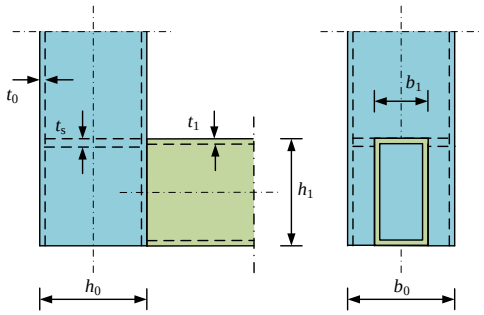

Connection KS

Floor beam-column joint

Geometrical information: b_0=140 mm, h_0=140 mm; b_1=80 mm; h_1=140 mm; $\beta=b_1/b_0$=0.57;$\eta=h_1/b_0$=1; $t_0=t_1$=8mm ; t_s=16 mm;

Physical information: f_y=355 Mpa; $m_0=f_y t_0^2/4$=5.68 kN=m_1 ; E=210000 Mpa; G=80769 Mpa

Column face bending (cfb):

$$M_{cfb}=m_0 h_1\left(\frac{1+\beta\, m_1/m_0}{\eta}+\frac{8\eta}{1-\beta}\right)=5.68\,kN\times 140\,mm\left(\frac{1+0.57\times 1}{1}+\frac{8\times 1}{1-0.57}\right)=\mathbf{16.1}\ (\text{kN}\cdot\text{m})$$

$$K_{cfb}=0.5k_{axail}(h_1-t_1)^2=0.5\frac{Et_0^3}{b_0^2}16\times\frac{t_1/b_0+(1-\beta)\tan(35-10\beta)}{(1-\beta)^3+10.4(1.5-1.63\beta)/(b_0/t_0)^2}(h_1-t_1)^2=\mathbf{2320}\ (\text{kN}\cdot\text{m})$$

Column side wall shear (cws):

$$A_v=2(h_0-t_0)t_0=2\times(140-8)\times 8=2112\ (\text{mm}^2)$$

$$M_{cws}=\frac{A_v(h_1-t_1)f_y}{\sqrt{3}}=\frac{1552\times(140-8)\times 355}{\sqrt{3}}=\mathbf{53.7}(\text{kN}\cdot\text{m})$$

$$K_{cws}=GA_v(h_0-t_1)=80769\times 2112\times(140-16)=\mathbf{11941}\ (\text{kN}\cdot\text{m})$$

Aggregated: $M_{FJ}=\min\{M_{cfb},M_{cws}\}=\mathbf{16.1}\ (\text{kN}\cdot\text{m})$ $\quad K_{FJ}=\dfrac{1}{\frac{1}{K_{cfb}}+\frac{1}{K_{cws}}}=\dfrac{1}{\frac{1}{2320}+\frac{1}{11940}}=\mathbf{1942}\ (\text{kN}\cdot\text{m})$

Ceiling beam-column joint

Geometrical information: b_0=140 mm, h_0=140 mm; b_1=80 mm; h_1=80 mm; $\beta=b_1/b_0$=0.57;$\eta=h_1/b_0$=0.57; $t_0=t_1$=8mm ;

Physical information: f_y=355 Mpa; $m_0=f_y t_0^2/4$=5.68 kN=m_1; E=210000 Mpa; G=80769 Mpa

Column face bending (cfb):

$$M_{cfb}=m_0 h_1\left(\frac{1+\beta\, m_1/m_0}{\eta}+\frac{8\eta}{1-\beta}\right)=5.68\,kN\times 80\,mm\left(\frac{1+0.57\times 1}{0.57}+\frac{8\times 0.57}{1-0.57}\right)=\mathbf{6.1}\ (\text{kN}\cdot\text{m})$$

$$K_{cfb}=0.5k_{axail}(h_1-t_1)^2=0.5\frac{Et_0^3}{b_0^2}16\times\frac{t_1/b_0+(1-\beta)\tan(35-10\beta)}{(1-\beta)^3+10.4(1.5-1.63\beta)/(b_0/t_0)^2}(h_1-t_1)^2=\mathbf{690}(\text{kN}\cdot\text{m})$$

Column side wall shear (cws):

$$A_v=2(h_0-t_0)t_0=2(80-8)\times 8=2112\ \text{mm}^2 \qquad M_{cws}=\frac{A_v(h_1-t_e)f_y}{\sqrt{3}}=\frac{2112\times(80-16)\times 355}{\sqrt{3}}=\mathbf{27.7}\ (\text{kN}\cdot\text{m})$$

$$K_{cws}=GA_v(h_0-t_e)=80769\times 2112\times(80-16)=\mathbf{6823}\ (\text{kN}\cdot\text{m})$$

Aggregated: $M_{CJ}=\max\{M_{cfb},M_{cws}\}=\mathbf{6.1}\ (\text{kN}\cdot\text{m})$ $\quad K_{CJ}=\dfrac{1}{\frac{1}{K_{cfb}}+\frac{1}{K_{cws}}}=\dfrac{1}{\frac{1}{690}+\frac{1}{6823}}=\mathbf{627}\ (\text{kN}\cdot\text{m})$

Column-Column joint

Geometrical sizes: L_{bolt}=230 mm, d=20 mm, A_{bolt}=314 mm^2

$$F_t=f_{y,bolt}A_{bolt}=640\times 314=201\ (\text{kN})$$

$$M_{VC}=\frac{f_{yb}A_b(h_0-t_0)}{2}=640\times 314\times\frac{(140-8)}{2}=\mathbf{13.3}\ (\text{kN}\cdot\text{m})$$

$$k_t=\frac{EA_{bolt}}{L_{bolt}}=210000\times\frac{314}{230}=287(\text{kN/mm})$$

$$K_{VC}=k_t[(h_0-t_0)/2]^2=287\times\left[\frac{(140-8)}{2}\right]^2=\mathbf{1249}\ (\text{kN}\cdot\text{m})$$

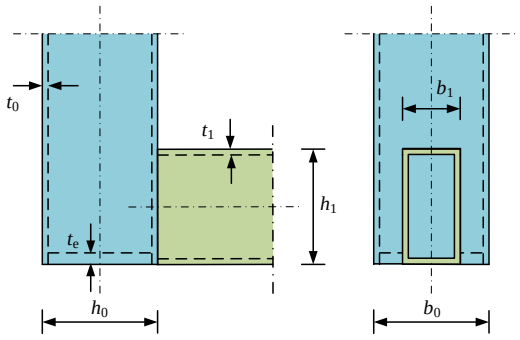

Connection BE

Floor beam-column joint

Geometrical information: b_0=140 mm, h_0=140 mm; b_1=80 mm; h_1=140 mm; $\beta=b_1/b_0$=0.57;$\eta=h_1/b_0$=1; $t_0=t_1$=8mm ; t_s=16 mm;

Physical information: f_y=355 Mpa; $m_0=f_y t_0^2/4$=5.68 kN=m_1 ; E=210000 Mpa; G=80769 Mpa

Column face bending (cfb):

$$M_{cfb}=m_0h_1\left(\frac{8}{\sqrt{1-\beta}}+\frac{8\eta}{1-\beta}+\frac{2}{\eta}\right)=5.68\times140\left(\frac{8}{\sqrt{1-0.57}}+\frac{8\times1}{1-0.57}+\frac{2}{1}\right)=\mathbf{26.2}(\text{kN}\cdot\text{m})$$

$$K_{cfb}=k_{axail}(h_1-t_1)^2=\frac{Et_0^3}{b_0^2}16\times\frac{t_1/b_0+(1-\beta)\tan(35-10\beta)}{(1-\beta)^3+10.4(1.5-1.63\beta)/(b_0/t_0)^2}(h_1-t_1)^2=\mathbf{4639}(\text{kN}\cdot\text{m})$$

Column side wall shear (cws):

$$A_v=(h_0-t_0-d)t_0+(h_0-t_0)t_0=(140-8-70)\times8+(140-8)\times8=1552\ (\text{mm}^2)$$

$$M_{cws}=\frac{A_v(h_1-t_1)f_y}{\sqrt{3}}=\frac{1552\times(140-8)\times355}{\sqrt{3}}=\mathbf{39.4}\ (\text{kN}\cdot\text{m})$$

$$K_{cws}=GA_v(h_1-t_1)=80769\times1552\times(140-8)=\mathbf{15544}\ (\text{kN}\cdot\text{m})$$

Aggregated: $M_{FJ}=\max\{M_{cfb},M_{cws}\}=\mathbf{26.2}(\text{kN}\cdot\text{m})$ $\quad K_{FJ}=\dfrac{1}{\frac{1}{K_{cfb}}+\frac{1}{K_{cws}}}=\dfrac{1}{\frac{1}{4639}+\frac{1}{15544}}=\mathbf{3573}\ (\text{kN}\cdot\text{m})$

Ceiling beam-column joint

Geometrical information: b_0=140 mm, h_0=140 mm; b_1=80 mm; h_1=80 mm; $\beta=b_1/b_0$=0.57;$\eta=h_1/b_0$=0.57; $t_0=t_1$=8mm ;

Physical information: f_y=355 Mpa; $m_0=f_y t_0^2/4$=5.68 kN=m_1; E=210000 Mpa; G=80769 Mpa

Column face bending (cfb):

$$M_{cfb}=m_0h_1\left(\frac{8}{\sqrt{1-\beta}}+\frac{8\eta}{1-\beta}+\frac{2}{\eta}\right)=5.68\times180\left(\frac{8}{\sqrt{1-0.57}}+\frac{8\times0.57}{1-0.57}+\frac{2}{1}\right)=\mathbf{12.0}(\text{kN}\cdot\text{m})$$

$$K_{cfb}=k_{axail}(h_1-t_1)^2=\frac{Et_0^3}{b_0^2}16\times\frac{t_1/b_0+(1-\beta)\tan(35-10\beta)}{(1-\beta)^3+10.4(1.5-1.63\beta)/(b_0/t_0)^2}(h_1-t_1)^2=\mathbf{1380}\ (\text{kN}\cdot\text{m})$$

Column side wall shear (cws):

$$A_v=2(h_0-t_0)t_0=2(80-8)\times8=2112\ \text{mm}^2 \qquad M_{cws}=\frac{A_v(h_1-t_1)f_y}{\sqrt{3}}=\frac{2112\times(80-8)\times355}{\sqrt{3}}=\mathbf{27.7}(\text{kN}\cdot\text{m})$$

$$K_{cws}=GA_v(h_1-t_e)=80769\times2112\times(80-16)=\mathbf{10917}\ (\text{kN}\cdot\text{m})$$

Aggregated: $M_{CJ}=\max\{M_{cfb},M_{cws}\}=\mathbf{12.0}\ (\text{kN}\cdot\text{m})$ $\quad K_{CJ}=\dfrac{1}{\frac{1}{K_{cfb}}+\frac{1}{K_{cws}}}=\dfrac{1}{\frac{1}{1380}+\frac{1}{10917}}=\mathbf{1225}\ (\text{kN}\cdot\text{m})$

Column-Column joint

Geometrical sizes: L_{bolt}=42 mm, d=20 mm, A_{bolt}=314 mm^2

$$F_t=f_{y,bolt}A_{bolt}=640\times314=201\ (\text{kN})$$

$$M_{VC}=\frac{f_{yb}A_b(h_0-t_0)}{2}=640\times314\times\frac{(140-8)}{2}=\mathbf{13.3}\ (\text{kN}\cdot\text{m})$$

$$k_t=\frac{EA_{bolt}}{L_{bolt}}=210000\times\frac{314}{42}=1570\ (\text{kN/mm})$$

$$K_{VC}=k_t[(h_0-t_0)/2]^2=1939\times\left[\frac{(140-8)}{2}\right]^2=\mathbf{6838}\ (\text{kN}\cdot\text{m})$$

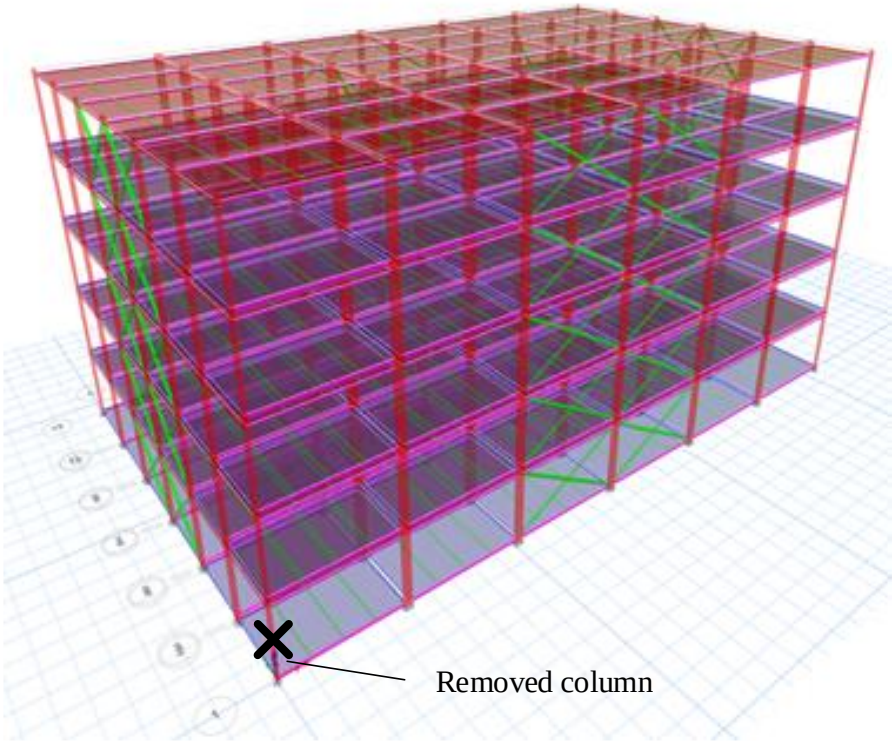

(a)

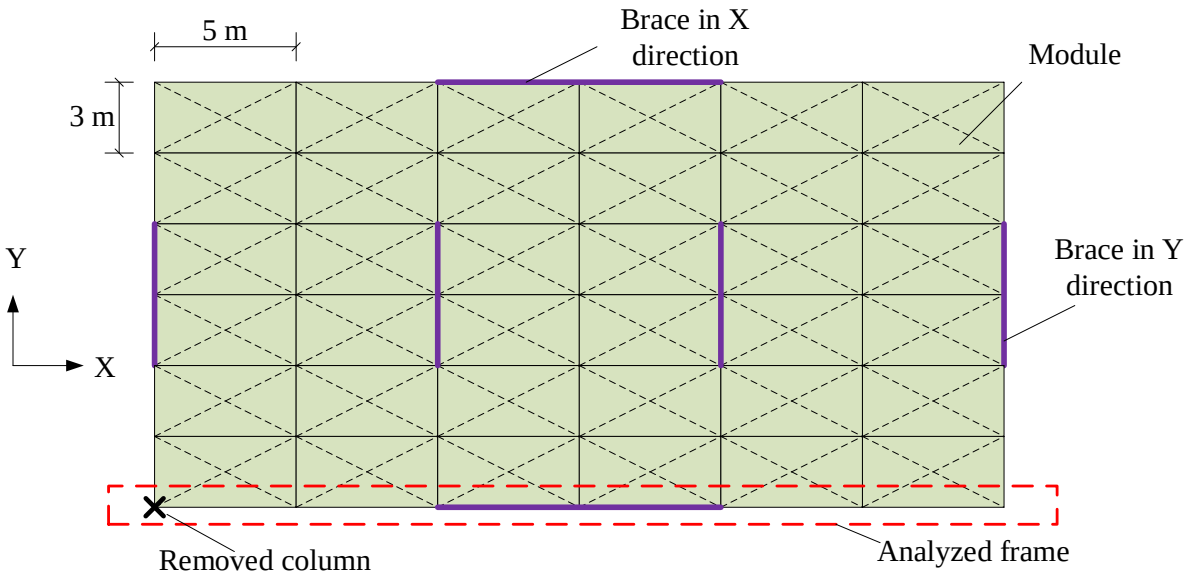

(b)

Figure 1. A steel MiC building: (a) 3D view; (b) planar view

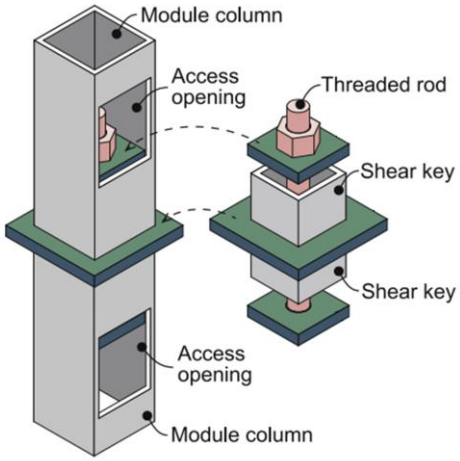

(a) Rod connection with shear key [25]

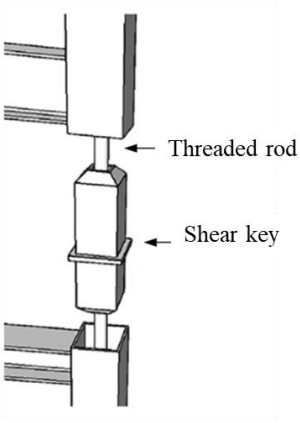

(b) Rod connection with shear key [24]

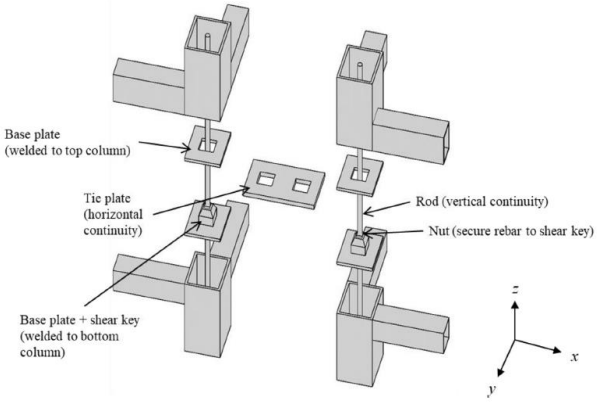

(c) Rod connection with shear key [12]

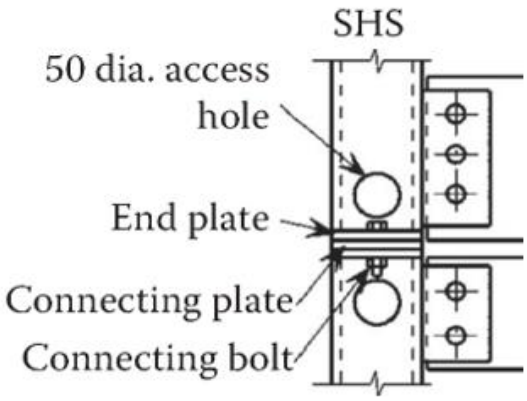

(d) Bolt connection [26]

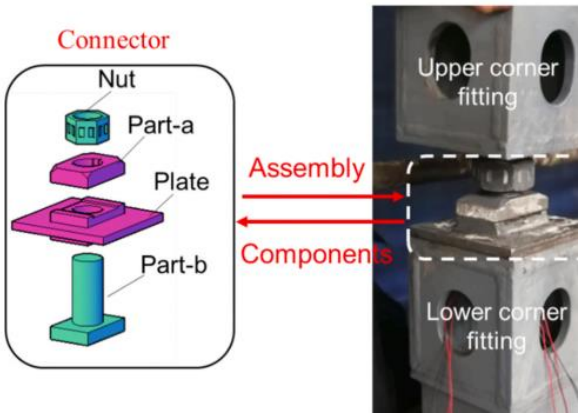

(e) Rod connection with shear key [12]

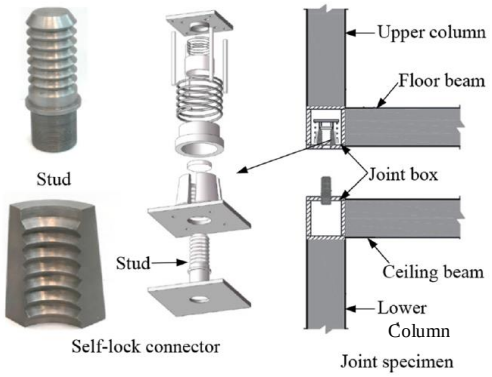

(f) Bolt connection [28]

Figure 2 Single rod/bolt inter-module connections

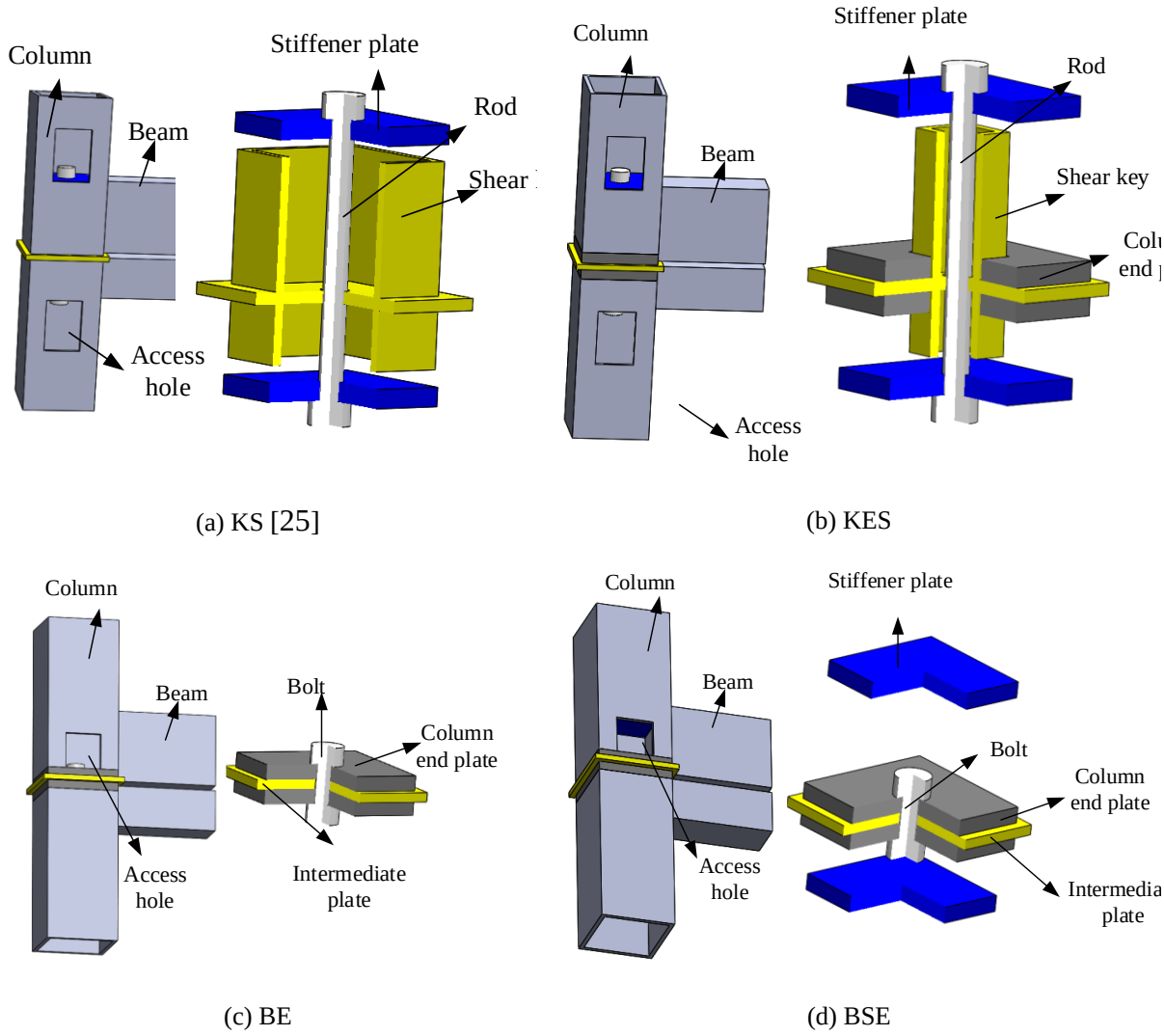

Figure 3 Four types of inter-module connections

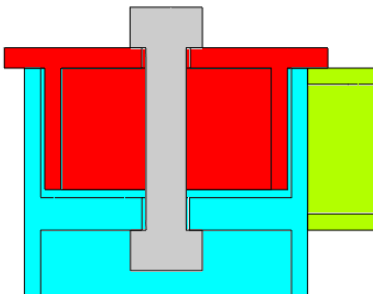

(a) External-Roof

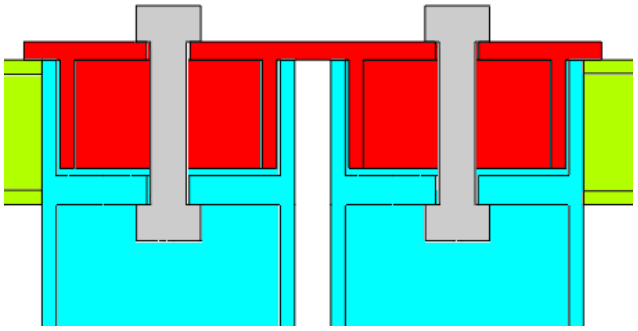

(b) Internal-Roof

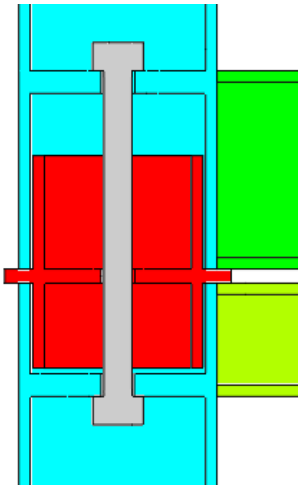

(c) External-Floor

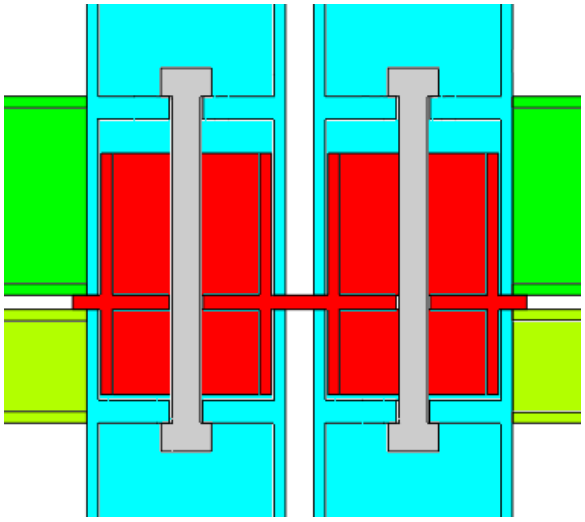

(d) Internal-Floor

Figure 4 Inter-module connections at different locations

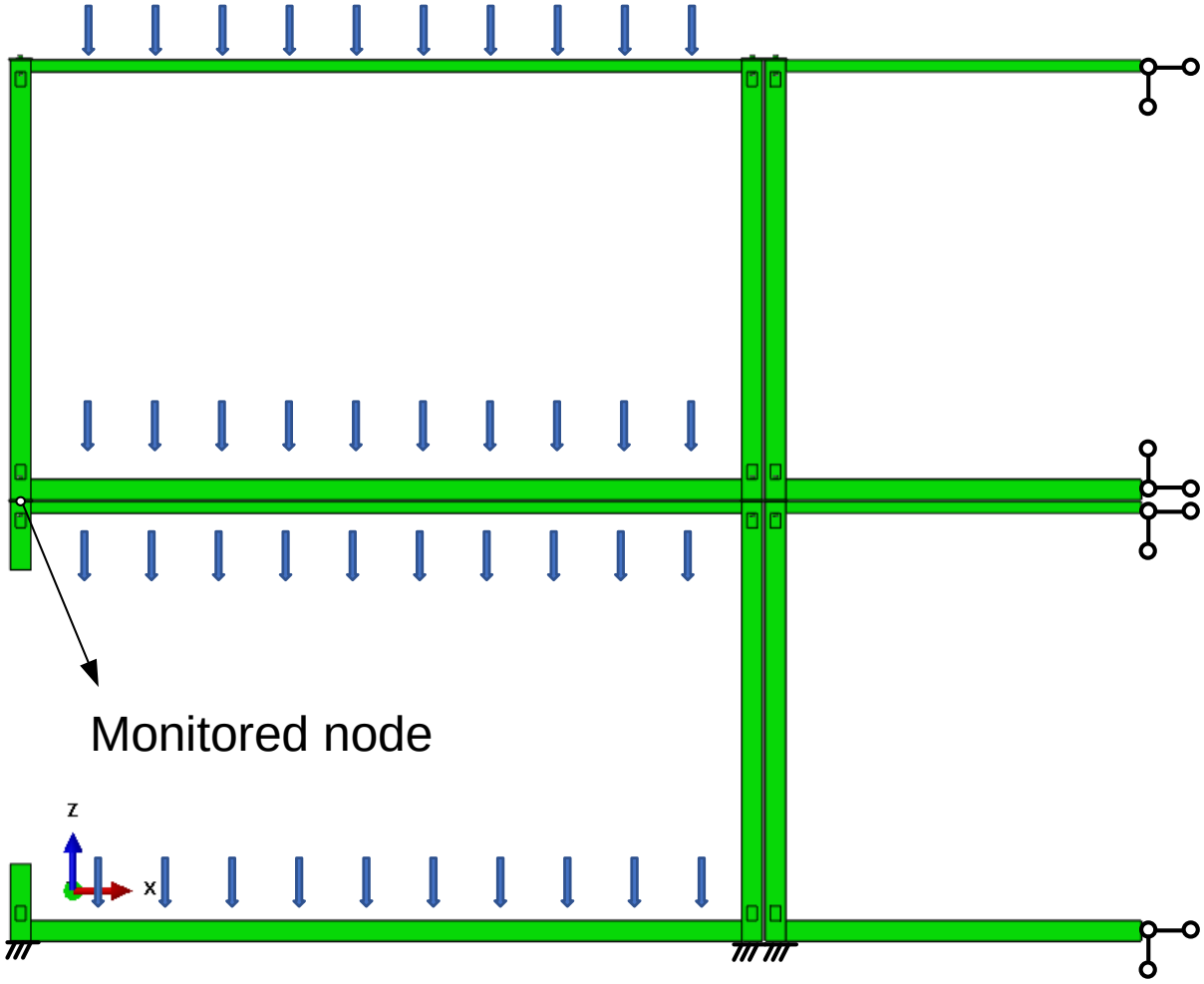

Figure 5 Sub-structure and loading configuration (connection KS)

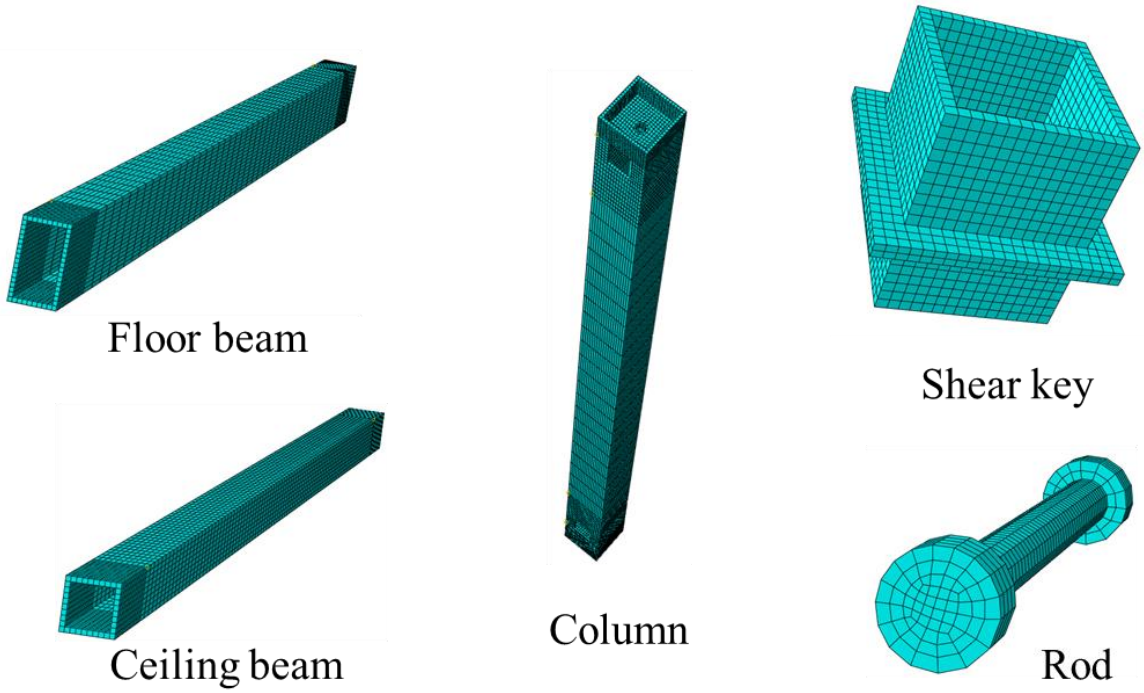

Figure 6 Mesh for components (connection KS)

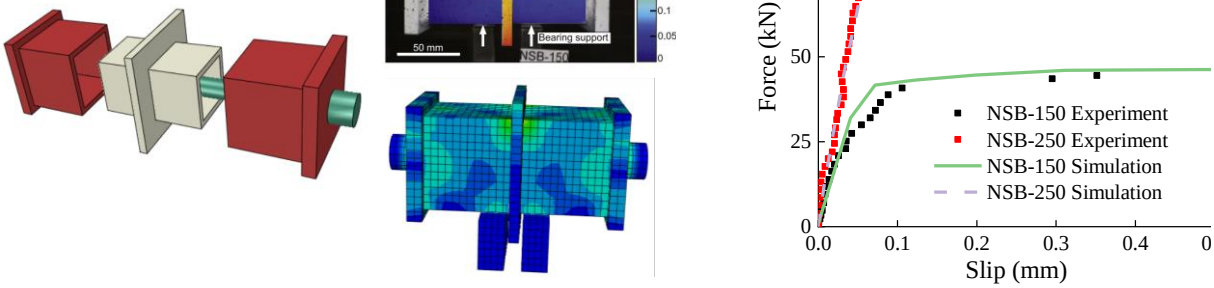

(a) Joint configuration

(b) Experimental and simulated deformation

(c) Force-slip curves for two specimens

Figure 7 Numerical vs. experimental comparison for slip tests ([25])

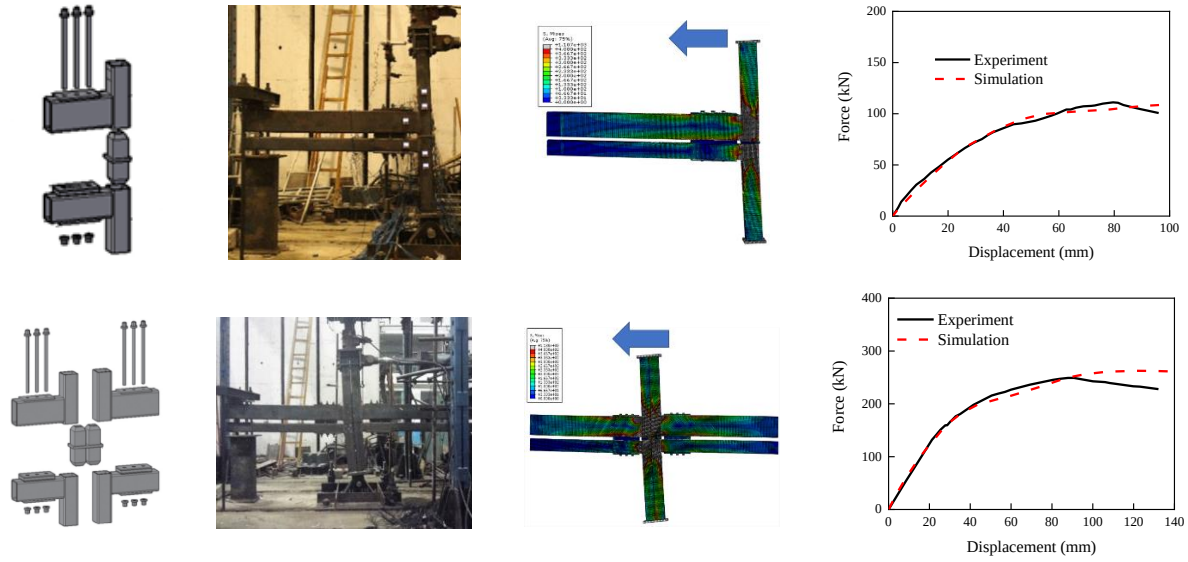

(a) Connection details

(b) Experimental global deformation

(c) Simulated global deformation

(d) Load-displacement curve

Figure 8 Numerical vs. experimental comparison for the external (upper) and internal (lower) inter-module connections under lateral loading [9, 10]

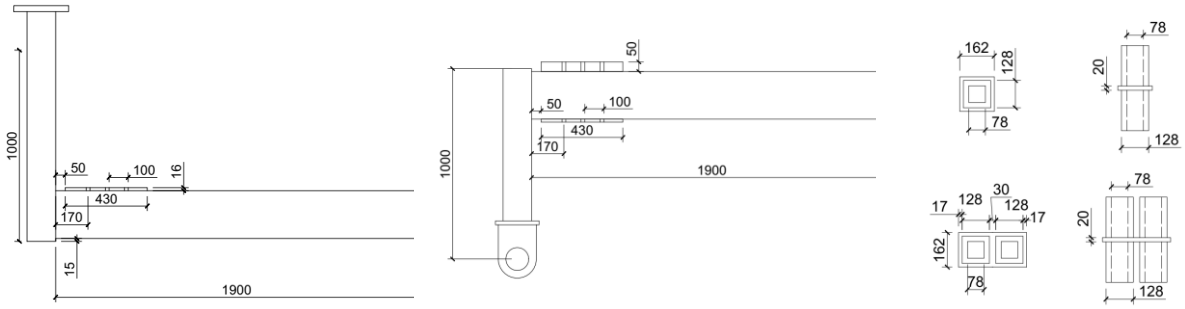

(a) Upper modular part

(b) Lower modular part

(c) Shear key for the external (upper) and internal (lower) connections

Figure 9 Dimension of the inter-module connections [9, 10]

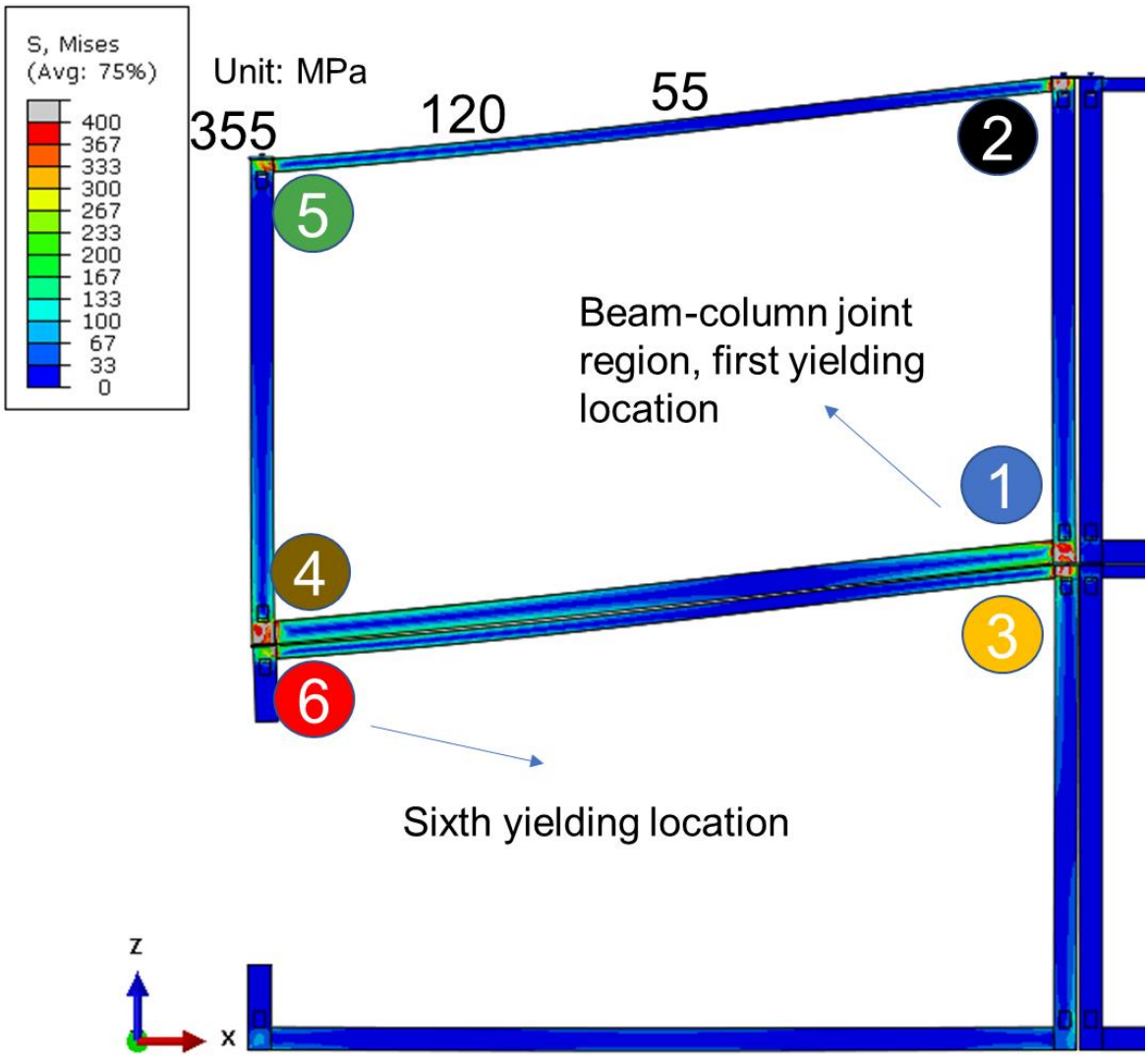

Figure 10 Global deformation at the final stage (vertical displacement of the monitored node equal to 0.1*L*) of the two-story sub-assemblage with shear key connection and yielding sequence (connection KS)

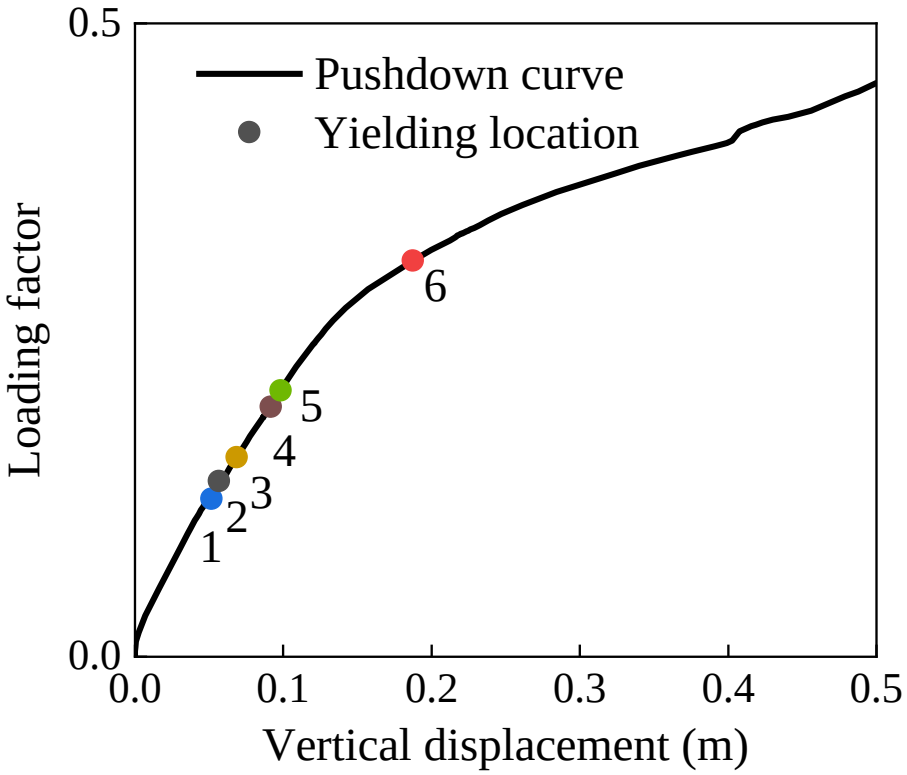

Figure 11 Load-displacement curve of the sub-structure with connection KS

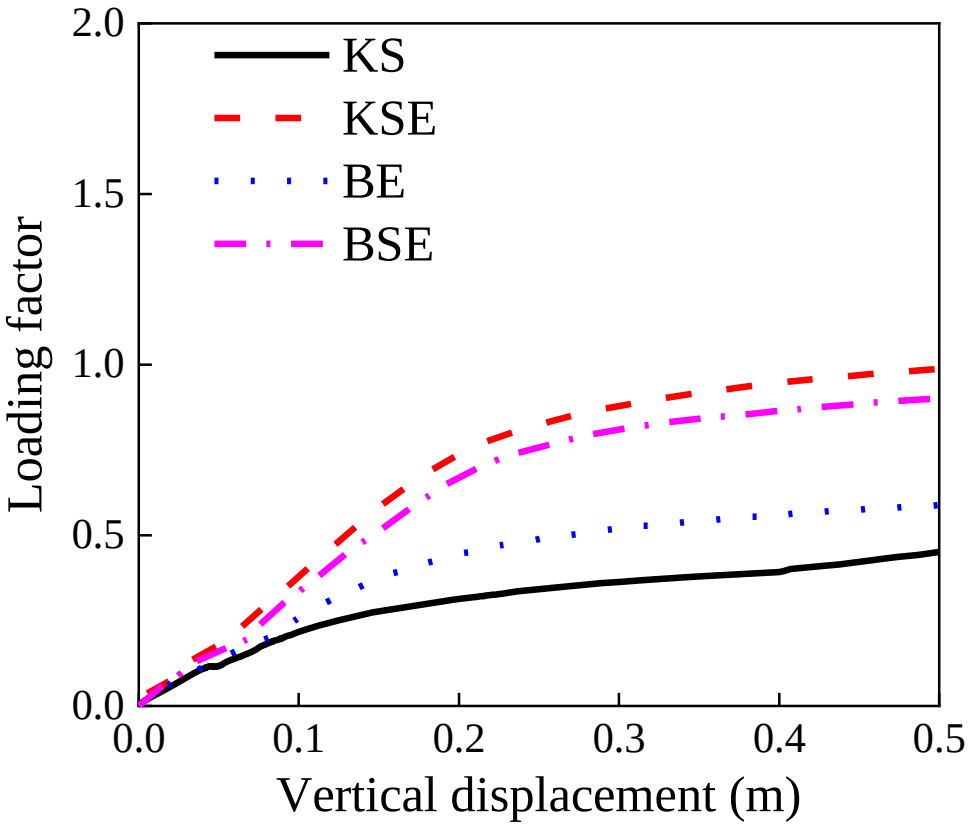

Figure 12 Load-displacement curve of the sub-structure with different types of connections

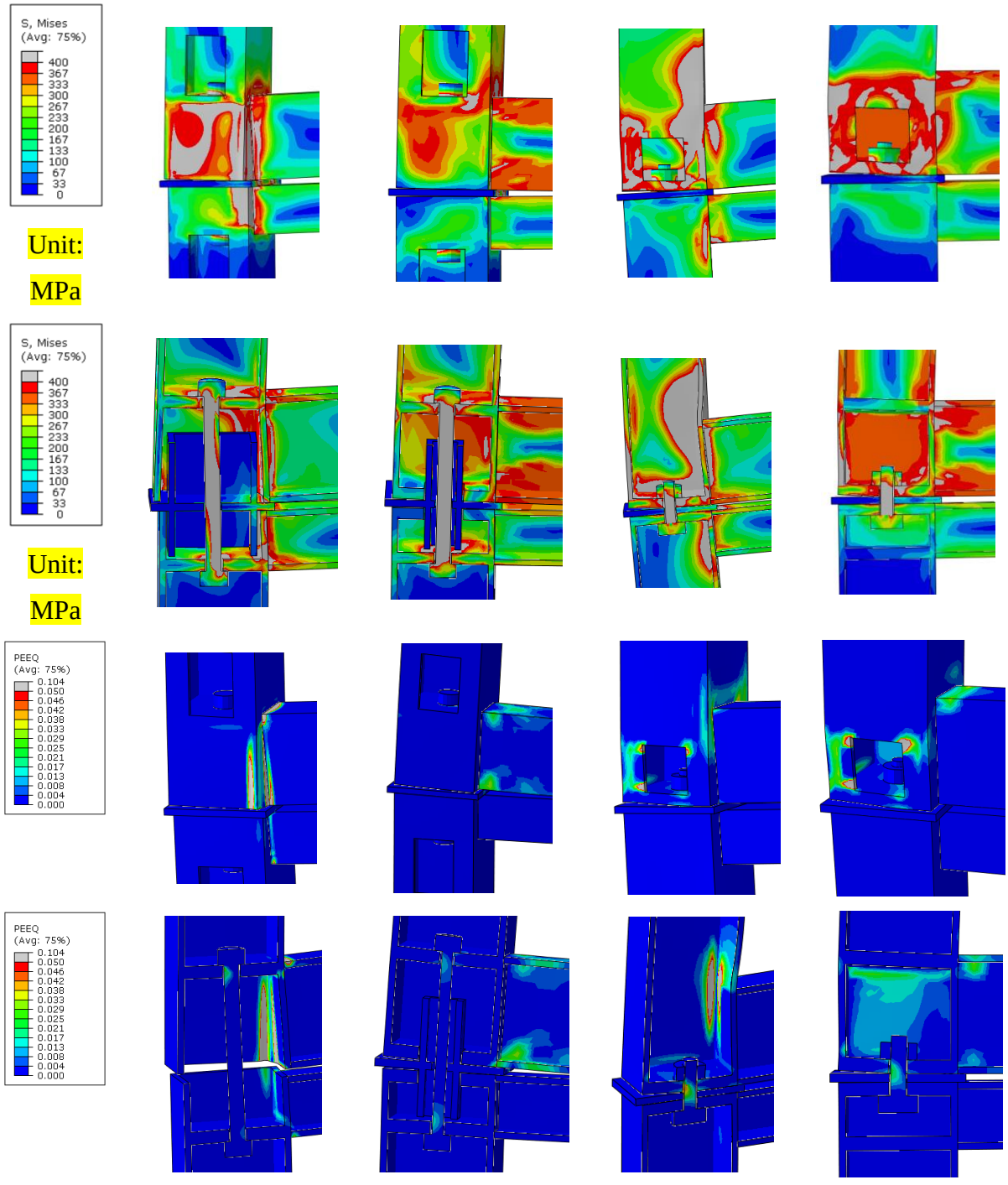

(a) KS (b) KSE (c) BE (d) BSE

Figure 13 Local deformation at the final stage (vertical displacement of the monitored node equal to 0.1*L*) at the external floor joint region with different connection types

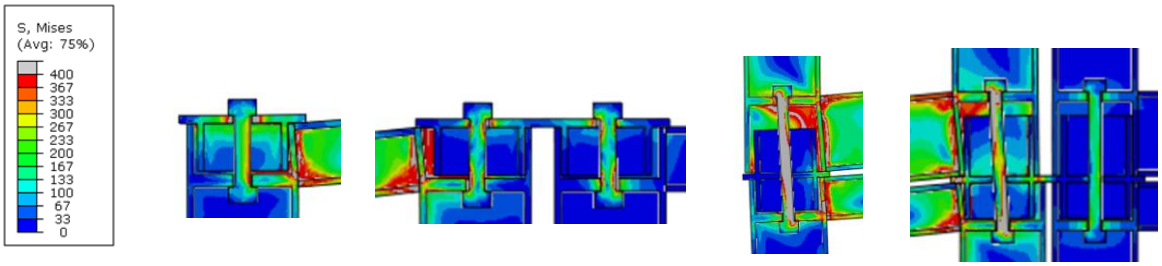

Unit: MPa

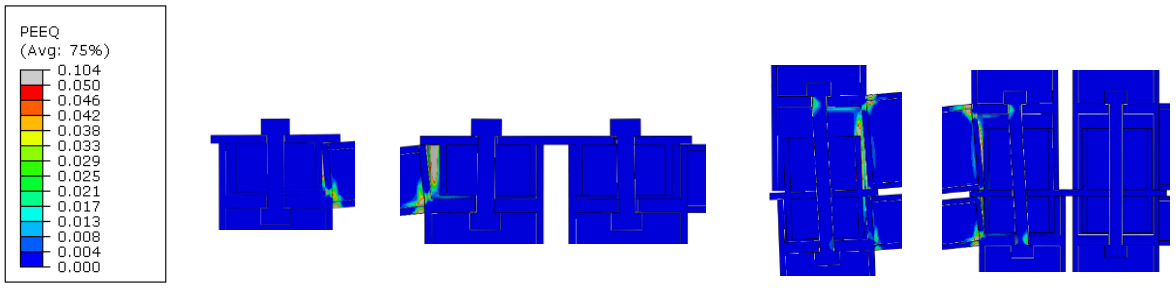

(a) External-Roof (b) Internal-Roof (c) External-Floor (d) Internal-Floor

Figure 14 Local deformation at the final stage (vertical displacement of the monitored node equal to 0.1*L*) for the connection KS at different locations

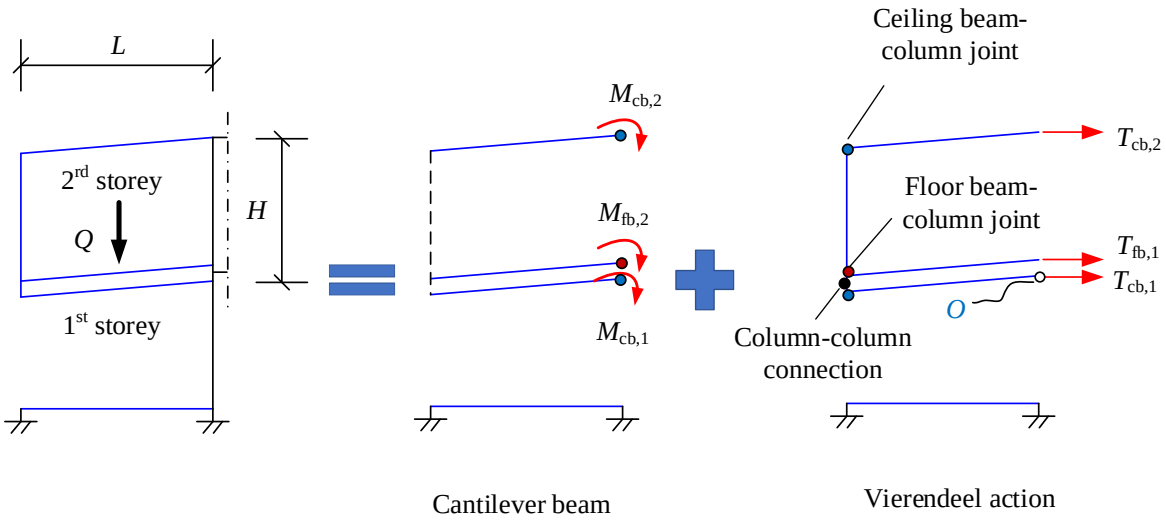

Figure 15 Load resisting mechanism under corner column removal scenario

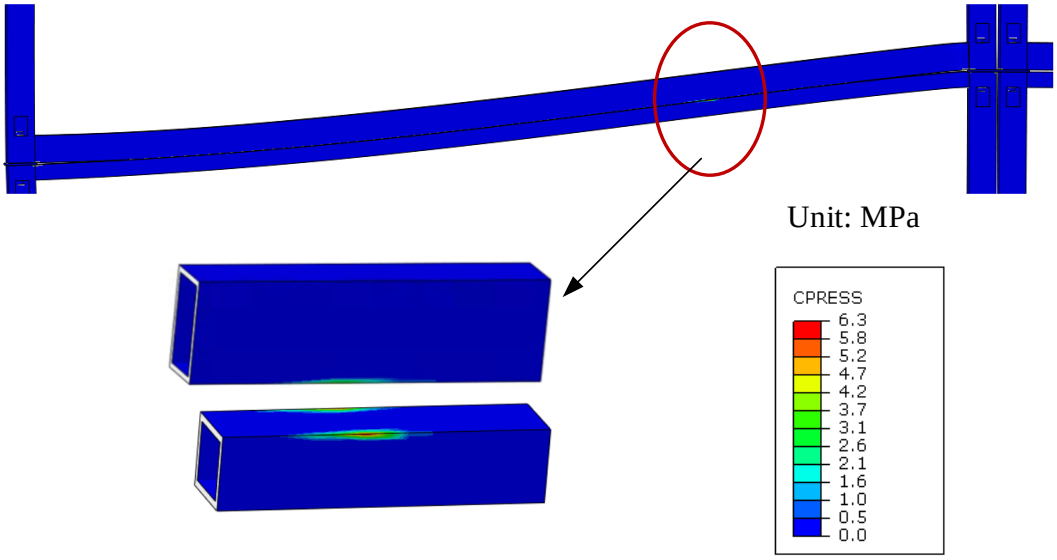

Figure 16 Contact stress on the ceiling beam (Unit: MPa) (Connection: KSE)

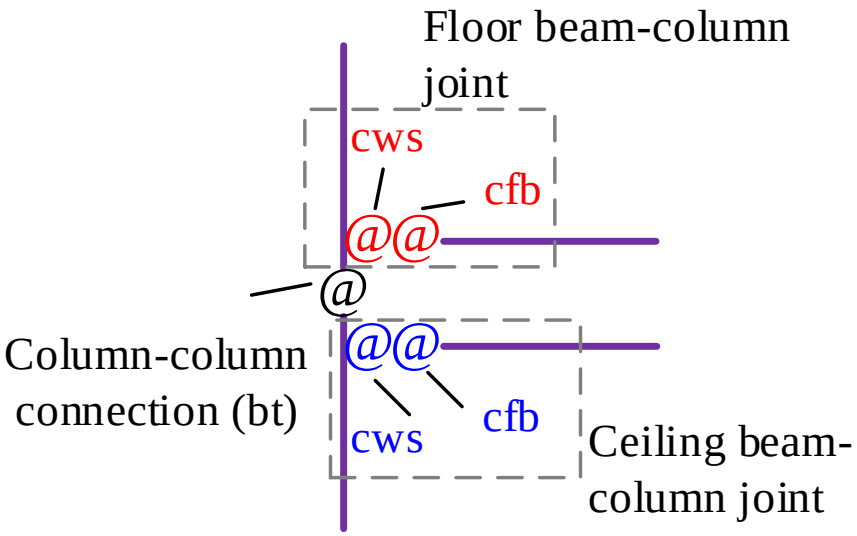

Figure 17 Simplified model for design

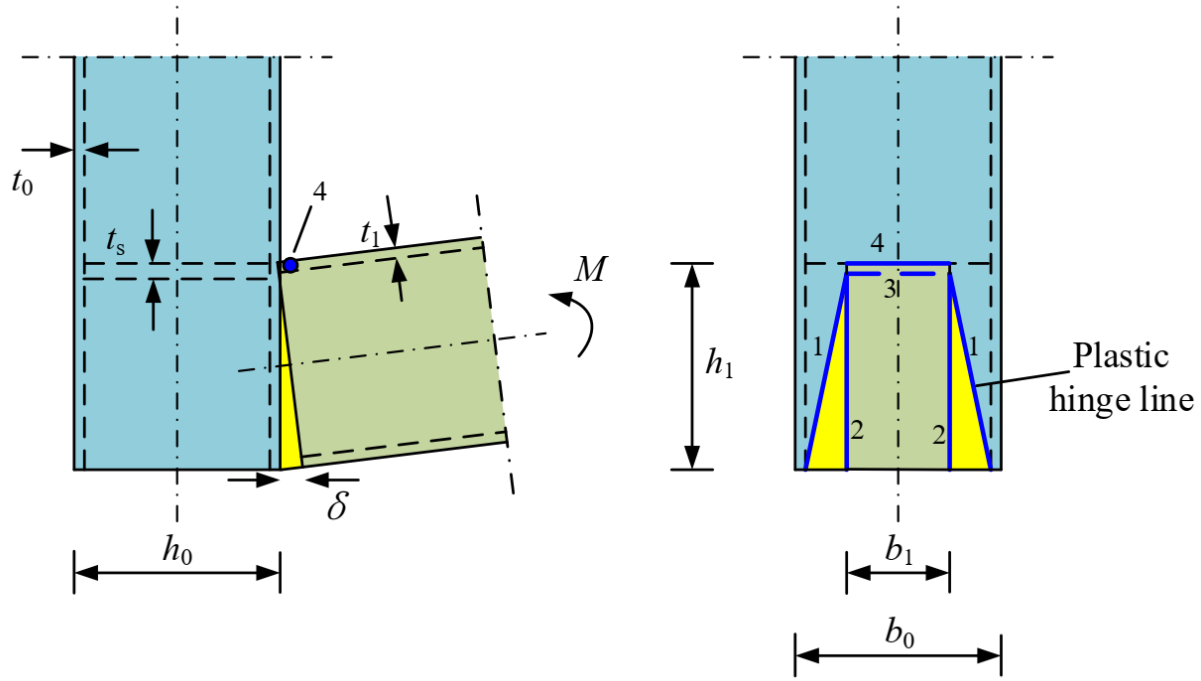

Figure 18 Geometrical information of KS connection and yield line of the shear key connection without endplate

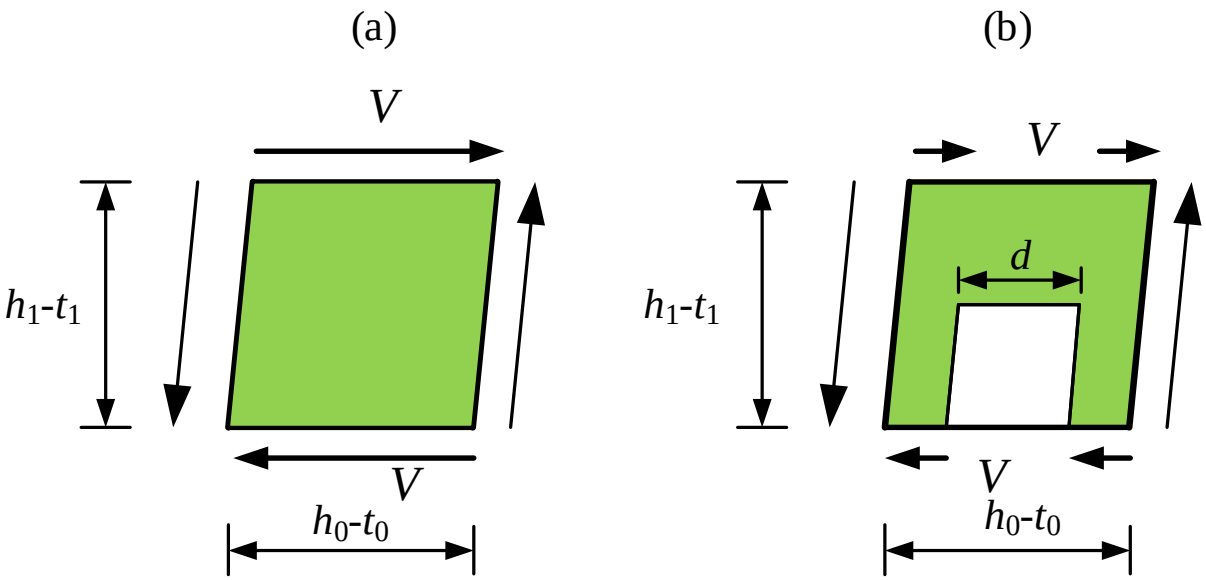

Figure 19 Model of the cws component: (a) without hole; (b) with hole.

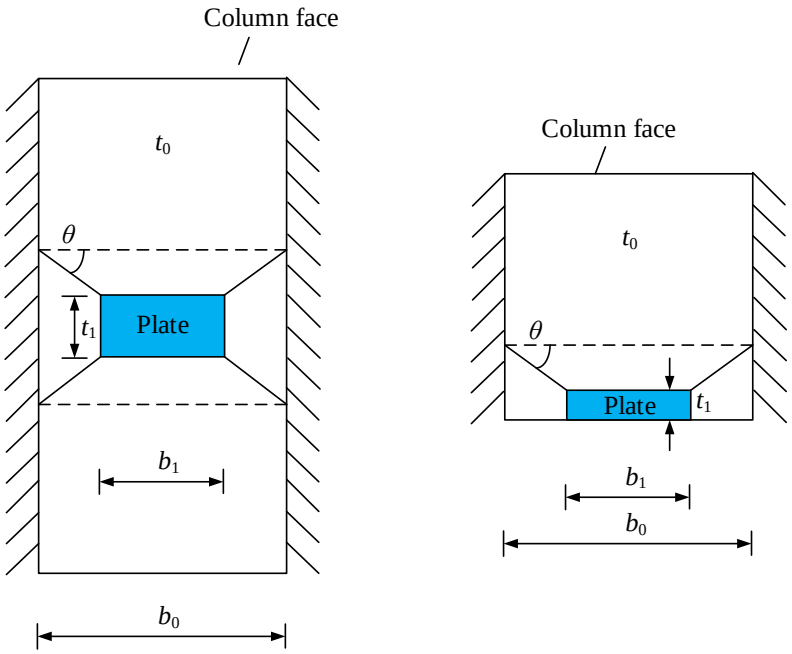

Figure 20 Axial stiffness model of rectangular plate to column face connection: (a) plate in the middle of column face [56]; (b) plate at the edge of column face - model for the column face in bending (cfb) component of connection KS

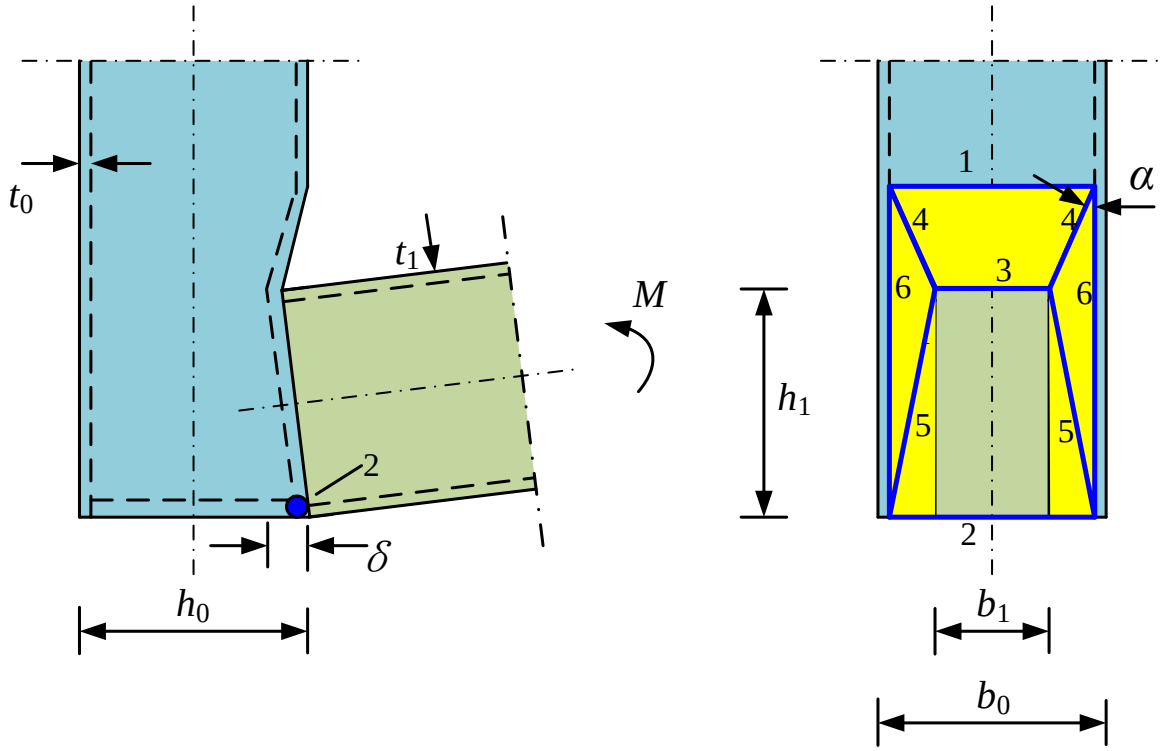

Figure 21 Yield line of the bolt connection without stiffener (BE)

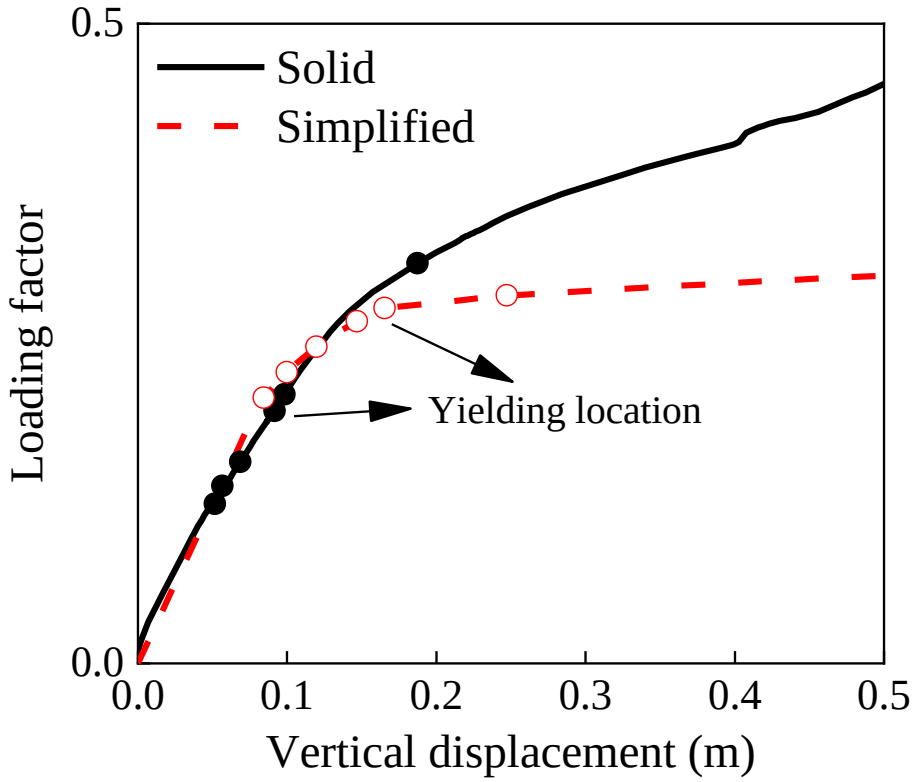

Figure 22 Load-displacement of the structure with simplified model using connection KS

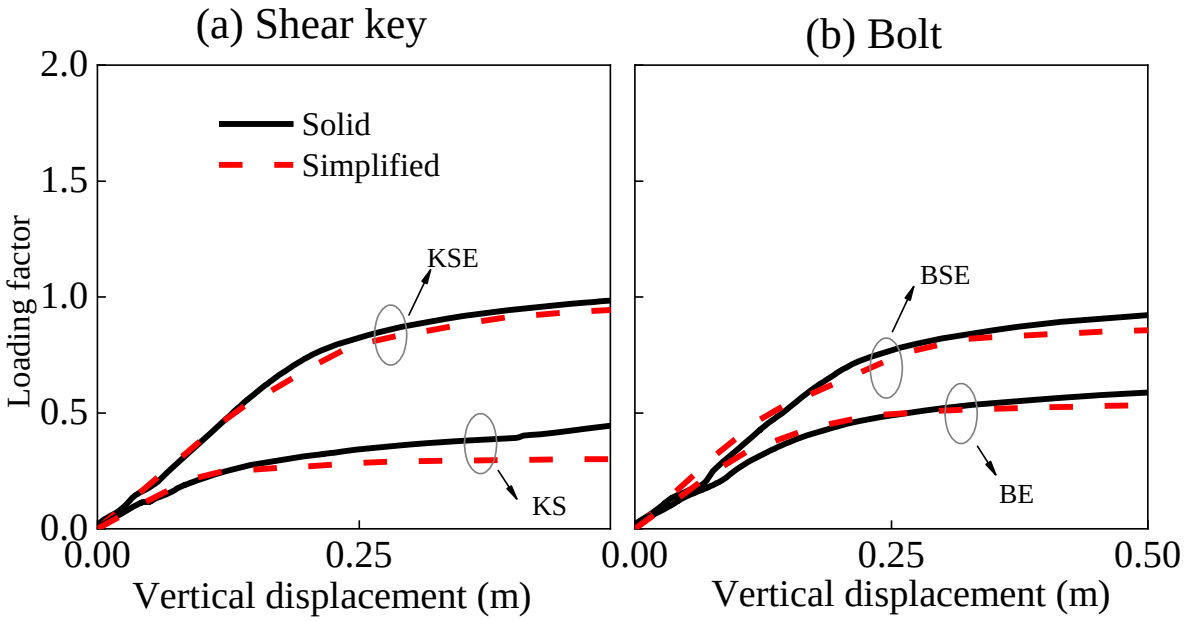

Figure 23 Load-displacement of the structure with simplified model

Table 1 Nominal loads in the building structure

	Dead load	Live load
Floor slab	4 kN/m^2	2 kN/m^2
Ceiling slab	2.25 kN/m^2	0 kN/m^2
Floor beam	5 kN/m	0 kN/m

Table 2 Section properties of elements

Member	Section size (mm)
Floor beams (X-direction)	RHS 140×80×8
Ceiling beams (X-direction)	RHS 80×80×8
Floor beams (Y-direction)	RHS 100×60×8
Ceiling beams (Y-direction)	RHS 80×80×6.3
Braces	L120×10
Columns	SHS 140×140×8

Table 3 Component sizes and material properties [9]

Component	Size (mm)	E (GPa)	f_y (MPa)	f_u (MPa)
Ceiling beam	150×150×8	210	425	575
Floor beam	150×250×8	210	425	575
Column	150×150×8	210	425	575
Shear key	See Figure 9	210	330	350

Table 4 Local failure modes at the joint region with different types of inter-module connections

Connection type	Failure modes
KS	(1) column face in bending (cfb)
KSE	No failure occurs at the joint region, but at beam ends
BE	(1) column face in bending (cfb), (2) column side wall in shear (cws), (3) bolt in tension (bt)
BSE	(1) column side wall in shear (cws), (2) bolt in tension (bt)

Table 5 Dissipated energy by yield lines for the shear key connection without endplate (KS)

Yield line	Internal energy	Internal energy (simplified)
1	$2m_0\left(\frac{\delta}{h_1}\frac{b_0-b_1}{2}+\frac{2\delta}{b_0-b_1}h_1\right)$	$2\left(\frac{1-\beta}{2\eta}+\frac{2\eta}{1-\beta}\right)m_0\delta$
2	$2m_0\left(\frac{2\delta}{b_0-b_1}h_1\right)$	$\frac{4\eta m_0\delta}{1-\beta}$
3	$m_0 b_1\frac{\delta}{h_1}$	$\frac{\beta m_0\delta}{\eta}$
4	$m_1 b_1\frac{\delta}{h_1}$	$\frac{\beta m_1\delta}{\eta}$

Table 6 Dissipated energy by the yield lines for the bolt connection without stiffeners (BE)

Yield line	Internal energy	Internal energy (simplified)
1	$b_0 m_0 \frac{2\delta \tan\alpha}{b_0 - b_1}$	$\frac{2\delta m_0 \tan\alpha}{1-\beta}$
2	$b_0 m_0 \frac{\delta}{h_1}$	$\frac{m_0 \delta}{\eta}$
3	$b_1 m_0 \left(\frac{2\delta \tan\alpha}{b_0 - b_1} + \frac{\delta}{h_1}\right)$	$\frac{2\delta\, \beta m_0 \tan\alpha}{1-\beta} + \frac{\beta\delta m_0}{\eta}$
4	$(b_0 - b_1) m_0 \frac{2\delta \tan\alpha}{b_0 - b_1} + 2\frac{b_0 - b_1}{2\tan\alpha} m_0 \frac{2\delta}{b_0 - b_1}$	$2\, m_0 \delta \tan\alpha + 2 m_0 \delta \cot\alpha$
5	$(b_0 - b_1) m_0 \frac{\delta}{h_1} + 2h_1 m_0 \frac{2\delta}{b_0 - b_1}$	$\frac{1-\beta}{\eta} m_0 \delta + \frac{4\eta m_0 \delta}{1-\beta}$
6	$2\left(h_1 + \frac{b_0 - b_1}{2\tan\alpha}\right) m_0 \frac{2\delta}{b_0 - b_1}$	$\frac{4\eta\delta m_0}{1-\beta} + 2 m_0\, \delta \cot\alpha$

Table 7 Stiffness and strength of connections (Unit: kN-m)

	KS		KSE		BE		BSE	
	Stiffness	Strength	Stiffness	Strength	Stiffness	Strength	Stiffness	Strength
Floor beam-column joint	1942 ($6EI/L$)	16.1 ($0.32M_B^*$)	11941 ($37EI/L$)	53.7 ($1.07M_B$)	3573 ($11EI/L$)	26.2 ($0.52M_B$)	15544 ($48EI/L$)	39.4 ($0.79M_B$)
Ceiling beam-column joint	627 ($8EI/L$)	6.1 ($0.29M_B$)	6823 ($86EI/L$)	27.7 ($1.31M_B$)	1225 ($15EI/L$)	12.0 ($0.57M_B$)	10917 ($137EI/L$)	27.7 ($1.31M_B$)
Column-column connection	1249	13.3	1249	13.3	6838	13.3	6838	13.3

*The moment capacities of the floor beam and ceiling beam, denoted as M_B in this table, are 50 and 21 kN-m, respectively; and the relative stiffness of floor beam and ceiling beam are 326 kN-m and 80 kN-m, respectively.